

The relationship between alpha burst activity and the default mode network

Mateusz Rusiniak^{1*}, Andrzej Wróbel², Katarzyna Cieśla¹, Agnieszka Pluta¹, Monika Lewandowska¹, Joanna Wójcik¹, Piotr H. Skarżyński³ and Tomasz Wolak¹

¹ Bioimaging Research Center, World Hearing Center of the Institute of Physiology and Pathology of Hearing, Warsaw/Kajetany, Poland, ² Department of Neurophysiology, Nencki Institute of Experimental Biology, Warsaw, Poland, ³ World Hearing Center of the Institute of Physiology and Pathology of Hearing, Warsaw/Kajetany, Poland

*Email: mateusz.rusiniak@gmail.com

Alpha rhythm, described by Hans Berger, is mainly recorded from the occipital cortex of relaxed subjects with their eyes closed. Early studies indicated the thalamo-cortical circuit as the origin of alpha rhythm. Recent works suggest an additional relationship between alpha rhythm and the Default Mode Network (DMN). We simultaneously recorded EEG and fMRI signals in 36 young males asked to alternately close and open their eyes in 30-s blocks. Using an EEG source channel montage (the recorded signal was interpolated to designated source positions corresponding to certain brain regions) we found an alpha rhythm sub-activity composed of its intrinsic events, called alpha bursting segments (ABS). More ABS were observed on source channels related to the DMN than those located over the occipital cortex (OC). Similarly, both the beamformer source analysis and fMRI indicated that the specific ABS activity detected on the PCC (posterior cingulate cortex/precuneus) source channel was less related to the OC than to the DMN source channels. The fMRI analysis performed using the PCC-ABS as a GLM regressor indicated an increased BOLD signal change in DMN nodes – precuneus and prefrontal cortex. These results confirm the OC source of alpha activity and additional specific sources of ABS in the DMN.

Key words: alpha rhythm, EEG, fMRI, precuneus, DMN

INTRODUCTION

Alpha activity in human electroencephalography (EEG) has attracted considerable interest since it was first described by Berger (1929). It is widely accepted that activity within the alpha frequency band (8–13 Hz) appears in the occipital lobe(s) of awake, relaxed subjects with eyes-closed and becomes attenuated when subjects open their eyes or exert mental effort (Berger 1929, Niedermeyer 2005). The latter phenomenon is called the “Berger effect,” and the preceding alpha oscillatory episodes in the EEG signal are often called “Berger waves” (Bazanov and Vernon 2014).

In early animal studies, Bishop (1936) proposed that alpha rhythm originated from reverberating cor-

tico-thalamic activity. This hypothesis has been supported by numerous animal studies that concluded that alpha oscillations are generated in the occipital cortex and the visual thalamus (Contreras and Steriade 1997, Moruzzi and Magoun 1949, Lopes da Silva et al. 1973, Lopes Da Silva and Storm Van Leeuwen 1977, Steriade et al. 1993). However, we are still lacking clear evidence that findings from animal models can be directly applied to alpha oscillations recorded in humans.

Simultaneous recordings of EEG and functional magnetic resonance imaging (fMRI) signals have allowed for investigation of the neuronal correlates of Berger waves in humans with great temporal and spatial resolution. This approach was first used by Goldman and colleagues (2002) to study the genera-

tion of alpha rhythm in subjects resting supine with eyes-closed. These authors observed a correlation between an increase in occipital alpha power and a decrease in fMRI blood oxygenation level-dependent (BOLD) signals in the occipital, superior temporal, inferior frontal, and cingulate cortices and with an increased hemodynamic response in the thalamus. Other EEG-fMRI results supported this finding (DiFrancesco et al. 2008, Feige et al. 2005, Liu 2012, Moosmann et al. 2003, de Munck et al. 2007, Tyvaert et al. 2008). Interestingly, some published results seemed to confirm increases (Ben-Simon et al. 2008) or decreases (Goldman et al. 2002, Moosmann et al. 2003) of the BOLD signal in anterior brain regions together with increases of alpha EEG activity in frontal recordings, but these relationships were not discussed in detail by the authors.

The classical hypothesis assumes a thalamo-occipital origin of the alpha rhythm (Goldman et al. 2002, Laufs et al. 2006, Lopes da Silva et al. 1973). Here we operationally term this type of alpha activity “occipital alpha”. Some authors have, however, postulated more diffuse sources of alpha activation across many distributed brain regions (Başar et al. 1997, Schürmann et al. 2000). Likewise, the latest research suggests that alpha rhythm may be related to the default mode network (DMN) (Ben-Simon et al. 2008, Mantini et al. 2007, Mo et al. 2013, Scheeringa et al. 2012, Zhan et al. 2014), here referred to as “DMN alpha”. This is interesting, in that although both alpha rhythm and the DMN are believed to reflect similar physiological states, the relationship between them is still ambiguous. Finally, an interesting approach has been presented by Bonnard and colleagues (2016) who stimulated main nodes of the DMN – the medial prefrontal cortex (mPFC) and, to some extent, the superior parietal lobule (SPL) by transcranial magnetic stimulation (TMS) and demonstrated that both regions were involved in some kind of modulation of alpha rhythm.

Importantly, alpha activity is characterized by segments of stable frequency (Lansky et al. 1979). Bazanova and Vernon (2014) argued that the shape of these spindle-form segments (Livanov 1984) should be considered an equally important parameter of alpha activity as its frequency or amplitude. Because these segments were postulated to play an important role in brain processing (Bazanova and Vernon 2014, Cole and Voytek 2017, Timofeev et al. 2002, Timofeev and Bazhenov 2005), we decided to analyze them in detail. Hereafter, they will be referred to as alpha bursting segments (ABS).

In the light of the latest findings, we reexamined Berger’s experiment – in search for ABS in two possible brain systems, the occipital network and the DMN.

METHODS

Participants

Sixty young male adults were recruited for this study. They had no history of neuropsychiatric disorders or head injury. Subjects provided written informed consent prior to participation. The project was approved by the Ethics Committee of the Institute of Physiology and Pathology of Hearing and conformed to the Declaration of Helsinki for Medical Research Involving Human Subjects.

Data from 9 subject were excluded because of movement exceeding 1.5 mm during the experiment. Additionally, 15 subjects were excluded from further analysis for several reasons based on visual inspection of the data. Some subjects fell asleep during recording (they did not open their eyes during the “eyes-open” condition, indicated by absence of blinking in EEG data), the EEG signal of others was distorted by non-reducible artifacts, and six subjects had no noticeable alpha frequency peak in FFT analysis [for more details on low-voltage EEG phenotype (see: Anokhin et al. 1992)]. In the remaining group (n=36), the mean age was 27 years \pm 4 years and 2 months.

Handedness was assessed using the Edinburgh Handedness Inventory (Oldfield 1971), and there were 17 right-handed, 18 left-handed, and 1 ambidextrous subjects. The handedness effect on EEG and fMRI results was verified to be negligible in this subject group (Rusiniak et al. 2014).

Experimental design

The study was performed during morning hours between 8 a.m. and noon. Prior to the EEG-fMRI experiment, all subjects were familiarized with the MR scanner environment. Before starting the fMRI session, we verified via an intercom that the subject felt comfortable and was relaxed. NordicNeuroLab goggles and headphones were used for visual and auditory stimulation, respectively.

Our implementation of the Berger experiment was similar to that described by Ben-Simon and colleagues (2008). Each subject was instructed to rest wakefully while alternately keeping their eyes closed or open (30 s for each block). The study started with an eyes-open block during which a black cross was centered on a grey background. The subject was asked to relax with eyes-open until the screen changed to black. After 30 s, a sound (a 0.5 s tone of 500 Hz, 80 dB) informed the subject to open his eyes, and the next block started. At the same time the screen for the eyes-open condition ap-

peared. These 2 block types were repeated 6 times, for a total of 12 blocks, resulting in approximately 6 min of the total paradigm time.

EEG signals: recording and preprocessing

EEG recordings were obtained using the Neuroscan SynAmpS system with a 64-electrode (10/10 system) Maglink cap. Two bipolar electrodes (vertical electro-oculogram [VEOG] and electrocardiogram [ECG]) were used for the purpose of artifact occurrence designation. The skin to electrode (sintered Ag/AgCl) impedance was kept below 15 k Ω for all electrodes. The signal was recorded continuously with a 10-kHz sampling rate. The clock synchronization between the MR scanner hardware and the EEG system was assured by a Neuroscan MRI/EEG Clock Synchronization Unit. During recording, the reference electrode was placed at CPz (recomputed afterwards to an average reference), and the FCz position was set as the ground electrode. We did not find any effect of the EEG equipment on fMRI outcomes during the quality assurance test.

Removal of fMRI gradient artifacts

The first step of the EEG signal analysis was removal of electrical artifacts induced by the MRI scanner gradient coils. High-voltage distortions caused by magnetic field fluctuations were removed by subtracting a moving averaged artifact waveform (averaged artifact samples=16) (Allen et al. 2000) based on the assumption that the subject did not move during registration (the maximum movement registered for each subject was <1 mm during the whole session).

Reduction of balistocardiogram

The balistocardiogram (BCG) was another source of EEG signal distortions that needed to be minimized (Debener et al. 2008). A direct ECG signal was collected with a bipolar ECG electrode placed on the subject's chest. We used a correlation-based algorithm implemented in BESA Research 6.1 (BESA GmbH, Gräfelfing, Germany) software to find R peaks in the QRS complex detected at this electrode. Next, a global-averaged artifact signal was created. A principal component analysis (PCA) was then performed on the averaged signal. A number of components (4 to 6, depending on the subject) were selected to obtain the artifact topography and reduce the influence of the BCG on the signal using the adaptive spatial filtering approach described by Ille and colleagues (2002) and implemented with BESA Research 6.1 software. This method of artifact filtering was sim-

ilar to that described in our previous paper (Rusiniak et al. 2013). Finally, the EEG signal was filtered using a band-pass filter (finite impulse response [FIR]) with a zero-phase shift, cut-off frequencies at 1–20 Hz, 12 dB/oct slope, and re-referenced to an average reference. In addition, the data were resampled at 100 Hz to accelerate further computation.

Source channel montage and the ABS detection algorithm

For the purpose of ABS detection one of the resting state montages, the 'DMN with Noise Sources' montage, was used (see Fig. S1) as implemented in BESA Research 6.1. This source channel montage consisted of 12 regional source channels from which six source channels were selected for further analysis (black circles in Fig. S1): PCC (posterior cingulate cortex), mPFC, LAG (Left Angular Gyrus), RAG (Right Angular Gyrus), LOCC (Left Occipital Cortex), ROCC (Right Occipital Cortex). First, four sources channels were located in brain regions that would explain the EEG activity related to the DMN and the last two were the *so-called* noise sources that collected EEG activity in the occipital lobe that was not a part of the DMN. Each source channel was treated identically. The resulting data was exported to MATLAB. Because each regional source consisted of three dipoles with the same localization but orthogonal orientations, the main direction was calculated using PCA for each regional source channel independently. The pre-processed EEG signal was analyzed using an in-house algorithm that automatically detected ABS. The general workflow of this algorithm is presented in Fig. 1 and shortly described below (2.4.1–2.4.3). Hereafter we refer to ABS detected over a particular source channel with a subscript (e.g. PCC_{ABS} for an ABS detected over the posterior cingulate cortex/precuneus channel).

FFT computation and individual alpha frequency computation

We independently determined alpha frequency of alpha activity for each subject and each source channel following the individual alpha peak frequency method described by Klimesch (1993) and Angelakis (2004) with their colleagues. The individual alpha frequency was based on independent calculations of FFTs that encompassed all 30-s-long blocks of data where subjects had their eyes closed. Each FFT spectrum was smoothed using methods described by Garcia (2010). The frequency with the maximum amplitude in the FFT spectrum was further considered the individual alpha frequency for the particular subject.

Estimation of individual alpha wave amplitude

This step was used to complement the limitation of the FFT analysis which only decomposes the EEG signal into a sum of sinusoidal functions that are characterized by frequency, amplitude (or power) and phase. The peak amplitude of a particular frequency is not fully reflected in the spectral domain of a complex signal but is also determined by the neighboring frequency bands. Since ABS is a convolution of two frequencies a precise analysis of the ABS amplitude should be performed, preferably in the time domain. For this purpose, we created a six-period sinusoid template with frequency equal to individual alpha frequency. In cases when the alpha-shaped segment was longer than the template, the algorithm produced several consecutive detections.

For estimation of ABS amplitude the EEG signal was temporally filtered with a band-pass filter (5–15 Hz). A cross-correlation was then computed between the template and the signal. Next, we extracted segments of the EEG signal with the highest correlation coefficients (>0.9). The absolute value of each segment's extremum was determined, and the 75th percentile of all resulting values was selected as the individual alpha amplitude.

Final computation of the ABS template

For the computation of the final ABS-like template shape the sinusoidal template that was used for individual alpha amplitude estimation was convolved with a modulation (envelope) function: a sinusoid with a period equal to half of the template length and amplitude equal to individual alpha amplitude.

Raw EEG signals were filtered with a broad band-pass filter (1–20 Hz) and a cross-correlation analysis was performed again between the selected EEG source channel signals and the calculated ABS-like template. Here the correlation coefficient threshold was set at 0.75. The additional detection criterion was applied that the mean value of the amplitude module for each detected ABS is between 50% and 150% of the individual alpha amplitude. The algorithm produced a vector containing the exact starting time points of ABS on a given source channel.

ABS detection analysis

A numerical statistical analysis was performed in IBM SPSS 24 online version (<https://www.apponfly.com/en/>). A one-way ANOVA with repeated measurements was used to compare the effect of the source channel on individual alpha frequency and ABS detection through-

out the whole EEG-fMRI session. The Tukey post-hoc analysis was performed to calculate the full ABS detection rate.

We also performed a within-subject analysis of correlation between regions assuming that events at two different regions are related if the time shift between them is not higher than ± 100 ms (the 180° phase shift for frequency of 10 Hz). The correlation coefficients for each subject were averaged independently for all region pairs.

Additionally, the number of detected ABS within 3 second long bins (an equivalent of the volume acquisition time using fMRI sequence) was averaged across all subjects to show the dynamics of ABS activity.

Source analysis of ABS

The multiple source linearly constrained minimum variance beamformer (Gross et al. 2001) was computed

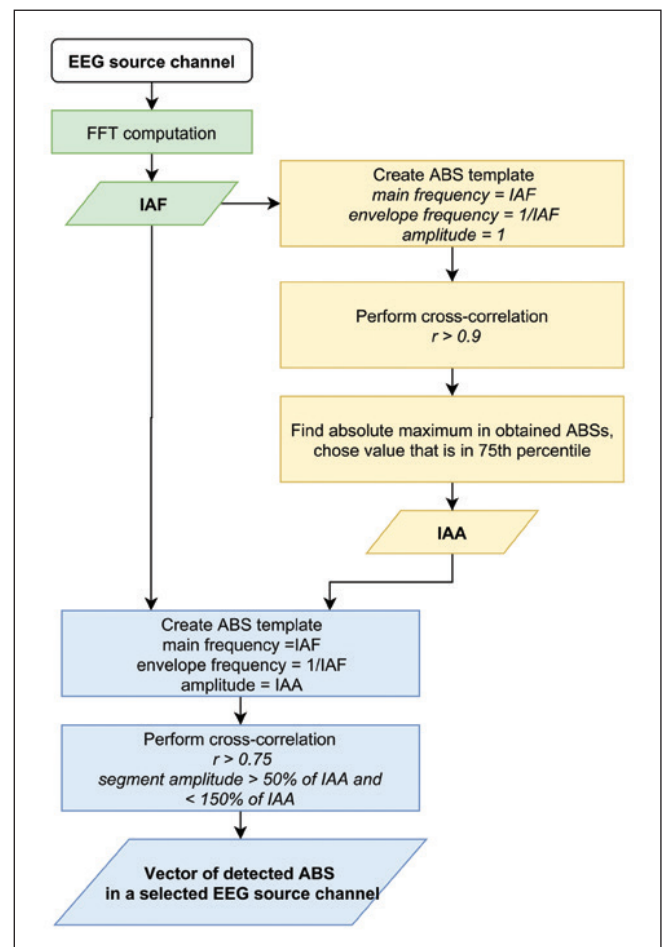


Fig. 1. Workflow of the ABS detection algorithm. The computation step searching for individual alpha frequency is marked with green, the assessment of individual alpha amplitude with yellow and the final computation part with blue.

for each subject as implemented in BESA Research 6.1 using average referenced data after postprocessing described in 2.3.

Prior to the source analysis a time-frequency analysis was performed. The EEG signal was epoched with respect to ABS start points. Each epoch interval started and ended 600 ms before and after the event marker. The beamformer analysis was performed for each subject and all ABS events obtained for the DMN source channels (PCC, mPFC, LAG, RAG). LOCC_{ABS} and ROCC_{ABS} events were combined because of an insufficient number of occurrences for a reliable beamformer computation. This result is hereinafter referred to as the occipital cortex ABS (OCC_{ABS}).

The ABS time frequency window was defined, covering the frequency range of 7–13 Hz and time range of 50–350 ms. The baseline was defined in an interval from (-600) to (-300) ms prior to the ABS marker. For source localization, the standardized FEM Model, as a realistic approximation for EEG, was used with default conductivity values approximated for adults (0.33 S/m for scalp and brain tissue, 0.0042 S/m for skull tissue, and 1.79 S/m for cerebrospinal fluid).

A group statistical comparison of the beamformer findings was performed in BESA Statistics 2.0 using a one-way ANOVA with repeated measurements. The obtained results were corrected for multiple comparisons

using a non-parametric permutation test with alpha cluster equal to 0.05 and 1000 permutations (corrected at $P < 0.001$).

fMRI image acquisition and analysis

To exclude subjects with brain pathology, standard T1 and T2 sequences were applied prior to functional imaging on a 3T MR scanner (Siemens Magnetom Trio TIM). Then EEG recordings were acquired simultaneously with fMRI data. A standard 12-channel matrix head coil was used for radiofrequency (RF) signal reception. The fMRI data were obtained using a T2*-weighted gradient echo-planar imaging sequence (repetition time 3000 ms, echo time 30 ms, flip angle 90°, image matrix 96 × 96, plane field of view 192 × 192 mm, integrated parallel acquisition techniques factor=2 with 42 ascending slices [slice thickness: 3 mm, no gap] parallel to the axial plane. There were 120 volumes (plus three extra dummy scans for steady-state magnetization) collected in the total scanning time of 6 min 11 s. A trigger signal was delivered by the MR scanner to the EEG recording system at each RF pulse.

The fMRI signal analysis was performed using Statistical Parametric Mapping software (SPM12, Wellcome Trust Centre for Neuroimaging, London, UK)

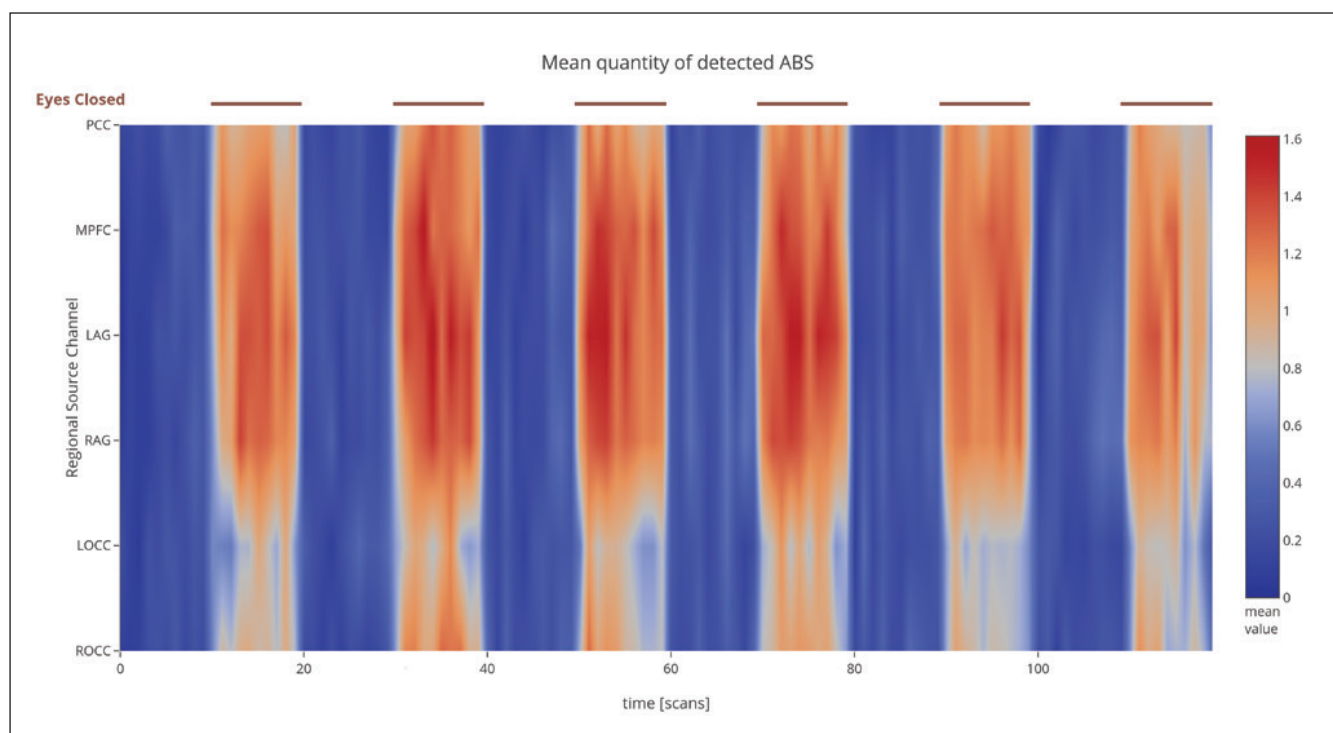


Fig. 2. The mean number of detected ABS in consecutive scans (3-s-long periods equal to the repetition time (TR) the fMRI sequence) averaged across all 36 participants. The ABS analysis was performed independently for each source channel. Note the increased number of ABS during the eyes-closed blocks (brown horizontal lines).

in MATLAB environment. Functional scans were pre-processed in the following steps: slice-time correction, head motion detection and correction, direct normalization to the Montreal Neurological Institute (MNI) space using ICBM152 EPI images, and spatial smoothing with an 8-mm FWHM Gaussian kernel. The data were also filtered in the temporal domain with a typical high-pass filter (128-s cut-off). The purpose of pre-processing was to remove various kinds of artifacts in order to maximize sensitivity of the following statistical analysis.

Since BOLD signal variance was dominated by fluctuations related to visual stimulation induced by the eyes-open condition, a more complex statistical parametric analysis was needed to reveal the ABS signal. Therefore, a general linear model (GLM) was created on the basis of a block-design paradigm (the eyes-open condition and the eyes-closed condition) and extended with event-related responses using an ABS-based vector (a separate GLM model for each ABS vector independently). ABS occurrences were modeled with the duration of stimuli equal to 0 (stick-function). The entire model was convolved with the canonical hemodynamic response function (HRF-double gamma functions), as implemented in the SPM12 package, to obtain final regressors for beta value calculation. Thus, our approach to data modeling was similar to that presented by Ben-Simon and colleagues (Ben-Simon et al. 2008), except for a different calculation of the alpha activity regressor (ABS was used instead of Ben-Simon's instantaneous alpha amplitude). The ABS-based regressor was compared with the eyes-closed condition. This contrast was chosen because ABS occurred mainly during eye closure (Fig. 2) whereas activity in occipital cortex characterized visual arousal during eyes-open. Contradicting regressor – eyes-closed – introduced to GLM minimized influence of visual input over fMRI data and allowed to verify whether ABS modulated brain activity also in the occipital area. Using this re-

gressor could, however, affect the sign of fMRI activity in occipital cortex. This issue will be discussed further in Discussion.

As this model did not fulfill the contrast orthogonality criterion for statistical parametric mapping an additional verification step was performed – we used the same GLM computation as above, but ABS vectors were randomly assigned to subjects.

The analysis was repeated for each ABS-based vector (PCC_{ABS} , $MPFC_{ABS}$, LAG_{ABS} , RAG_{ABS} , $LOCC_{ABS}$, $ROCC_{ABS}$, and OCC_{ABS}). This produced 7 independent outcomes. As the last step of the fMRI analysis, we performed a paired t-test comparing PCC_{ABS} and OCC_{ABS} . Here only ABS vectors were included in the GLM; the eyes-open and eyes-closed paradigm parameters were excluded to avoid beta deviation during model estimation.

All fMRI data analysis results, except for the paired t-test, were reported with cluster-level correction for multiple comparisons ($P < 0.05$) after passing an uncorrected threshold of $P = 0.001$ (AlphaSim correction for multiple comparisons; Ward 2000) (the minimum cluster size was set to 177 voxels of $2 \times 2 \times 2$ mm resulting in a volume of 1.416 cm^3). The outcomes of the paired t-test were reported with cluster-level correction for multiple comparisons ($P < 0.05$) after passing an uncorrected threshold of $P = 0.005$ (the minimum cluster size was set to 396 voxels of $2 \times 2 \times 2$ mm resulting in a volume of 3.168 cm^3).

RESULTS

ABS detection

ABS segments were mainly detected during the eyes-closed state (Fig. 2). A post-hoc analysis (Table I) showed that the mean number of ABS in $LOCC_{ABS}$ and $ROCC_{ABS}$ was much lower than in the DMN source channels, with statistically significant differences demon-

Table I. Difference between mean number (\bar{x}) of ABSs on source channel pairs over 36 subjects (ANOVA's Tukey post-hoc analysis). Significant values are colored.

		PCC_{ABS}	$MPFC_{ABS}$	LAG_{ABS}	RAG_{ABS}	$LOCC_{ABS}$	$ROCC_{ABS}$
PCC_{ABS}	($\bar{x}=75$)						
$MPFC_{ABS}$	($\bar{x}=86$)	-11.2					
LAG_{ABS}	($\bar{x}=90$)	-15.8	-4.6				
RAG_{ABS}	($\bar{x}=86$)	-11.5	-0.3	4.3			
$LOCC_{ABS}$	($\bar{x}=60$)	13.8	25*	29.6*	25.3*		
$ROCC_{ABS}$	($\bar{x}=68$)	6.6	17.9	22.4+	18.1	-7.1	

* significant result ($P < 0.05$); + trend toward significance ($P < 0.08$).

strated between $mPFC_{ABS}$ and $LOCC_{ABS}$ ($MD=25$, $P<0.05$), LAG_{ABS} and $LOCC_{ABS}$ ($MD=29.6$, $P<0.005$) and RAG_{ABS} and $LOCC_{ABS}$ ($MD=25.3$, $P<0.05$). This observation was supported by ANOVA results showing a main effect of source channel for ABS detection ($F_{5,210}=4.059$, $P=0.002$). Furthermore, inter subject correlation analysis (Table II) indicated a highly significant correlation between ABS detection rates of two opposite lateral DMN regions: LAG_{ABS} and RAG_{ABS} ($r=0.55$, $P<0.001$) and between $mPFC_{ABS}$ and LAG_{ABS} ($r=0.35$, $P<0.05$). ABS detection in regions that were not part of the DMN – $LOCC_{ABS}$ and $ROCC_{ABS}$ – were not correlated with any of the DMN regions, but correlated with one another ($r=0.34$, $P<0.05$). A weak correlation was observed between PCC_{ABS} and $mPFC_{ABS}$ ($r=0.22$) and $mPFC_{ABS}$ and RAG_{ABS} ($r=0.28$). There were no significant differences revealed between the selected source channels in terms of their individual alpha frequency ($F_{5,210}=0.21$, $P=0.96$).

EEG source analysis

ABS activity occurred mainly during the eyes-closed state (Fig. 2) and could not be differentiated from the occipital alpha rhythm by using only a typical frequency analysis. We already noted some differences between detection rates but this finding was not enough to imply that occipital alpha rhythm differs substantially from the DMN alpha rhythm.

A one-way ANOVA with repeated measurements was used to compare the effect of the source channel on beamformer source analysis (Fig. 3). This analysis revealed a main effect ($P<0.01$) in parietal regions (red cluster in top row of Fig. 3). There was also a less pronounced but a still significant effect ($P<0.05$) revealed in the dorsal part of the frontal lobe (orange cluster in Fig. 3). Note that beamformer analysis revealed sources in occipital cortex for both ABS_{PCC} (Fig. 3, middle row) and ABS_{OCC} (Fig. 3, bottom row),

but in parietal regions only sources related to ABS_{PCC} were present. A post-hoc analysis showed that the outcome of the beamformer analysis for OCC_{ABS} was significantly different when compared to the beamformer computation obtained for PCC_{ABS} ($P<0.05$, Fig. 4). A post-hoc analysis furthermore demonstrated very small clusters of difference when PCC_{ABS} was compared with LAG_{ABS} and RAG_{ABS} . These results were provided as supplementary materials (Figs S2 and S3, respectively).

fMRI results

To further assess the neural correlates of ABS, fMRI data were analyzed using a model-driven approach. We performed a GLM analysis of fMRI data using regressors derived from the two study conditions (eyes-open and eyes-closed) and temporal information of ABS occurrence obtained from EEG data (independently for all source channels – six plus one additional for combined $LOCC_{ABS}$ and $ROCC_{ABS}$). The result for PCC_{ABS} is presented in Fig. 5 and the result for OCC_{ABS} is presented in Fig. 6.

Regions that exhibited a significant positive correlation ($P<0.05$ AlphaSim corrected for multiple comparisons, after passing an uncorrected threshold of $P=0.001$) between the recorded BOLD signal and PCC_{ABS} were located in frontal, parieto-medial, and occipital clusters (Fig. 5, warm colors; Table SI). The frontal cluster included predominantly bilateral superior frontal gyri. The parieto-medial cluster comprised the precuneus and posterior parts of the cingulate gyri. The occipital cluster mainly consisted of bilateral areas including the calcarine fissures, lingual gyri, occipital gyri, fusiform gyri and cuneus. The frontal and parieto-medial clusters revealed by the described analysis corresponded to two main nodes of the DMN (i.e. the medial prefrontal cortex and the precuneus,

Table II. Within subject correlation coefficients of ABS detection between source channels pairs averaged over 36 subjects. Significant values are colored.

	PCC_{ABS}	$mPFC_{ABS}$	LAG_{ABS}	RAG_{ABS}	$LOCC_{ABS}$	$ROCC_{ABS}$
PCC_{ABS}						
$mPFC_{ABS}$	0.22					
LAG_{ABS}	0.14	0.35*				
RAG_{ABS}	0.12	0.28	0.55**			
$LOCC_{ABS}$	0.11	0.11	0.11	0.16		
$ROCC_{ABS}$	0.12	0.13	0.15	0.14	0.34*	

* significant result ($P<0.05$), ** highly significant result ($P<0.001$).

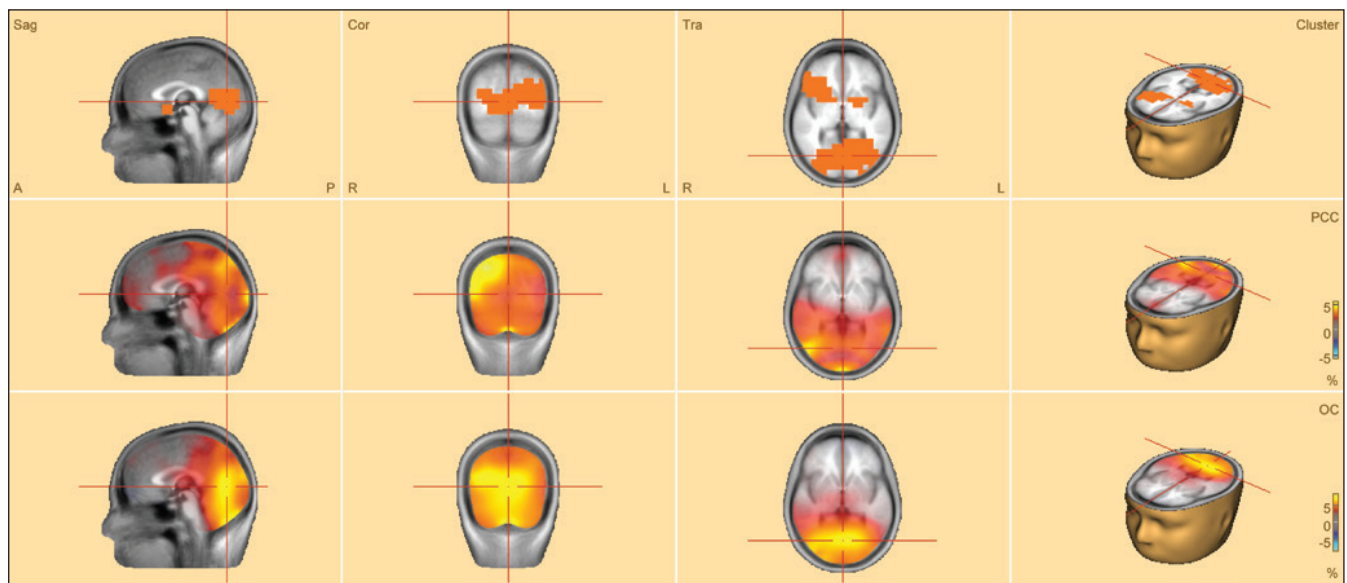


Fig. 3. Main effect of the ANOVA with repeated measurements analysis of beamformer source localization. The first row presents the clusters of significance (red cluster: $P < 0.01$, orange cluster: $P < 0.05$), the second row shows the EEG sources found by beamformer for PCC_{ABS} and the third row presents the result obtained for OCC_{ABS} .

alongside the posterior part of the cingulate gyrus), as described by Raichle and colleagues (Raichle et al. 2001). In addition, the analysis revealed lateral regions with a negative correlation between the GLM model and the acquired BOLD signal changes (Fig. 5, cold colors). The lateral cluster consisted predominantly of bilateral rolandic operculi, postcentral gyri and temporal gyri.

The result of the analysis where OCC_{ABS} was implemented in GLM showed very similar results in terms of anatomical locations but with some important dif-

ferences. The occipital cluster as well as both lateral clusters covered larger areas and reached higher absolute values of t-statistics. The revealed frontal cluster was much smaller and the parieto-medial cluster was not present at all. A new fronto-medial cluster was detected, comprising the middle part of the cingulate gyri.

Detailed information on the brain regions presented in Fig. 5 are specified in supplementary Table SI. The results obtained for the remaining source channels ($mPFC_{ABS}$, LAG_{ABS} , RAG_{ABS} , $LOCC_{ABS}$ and $ROCC_{ABS}$) are pro-

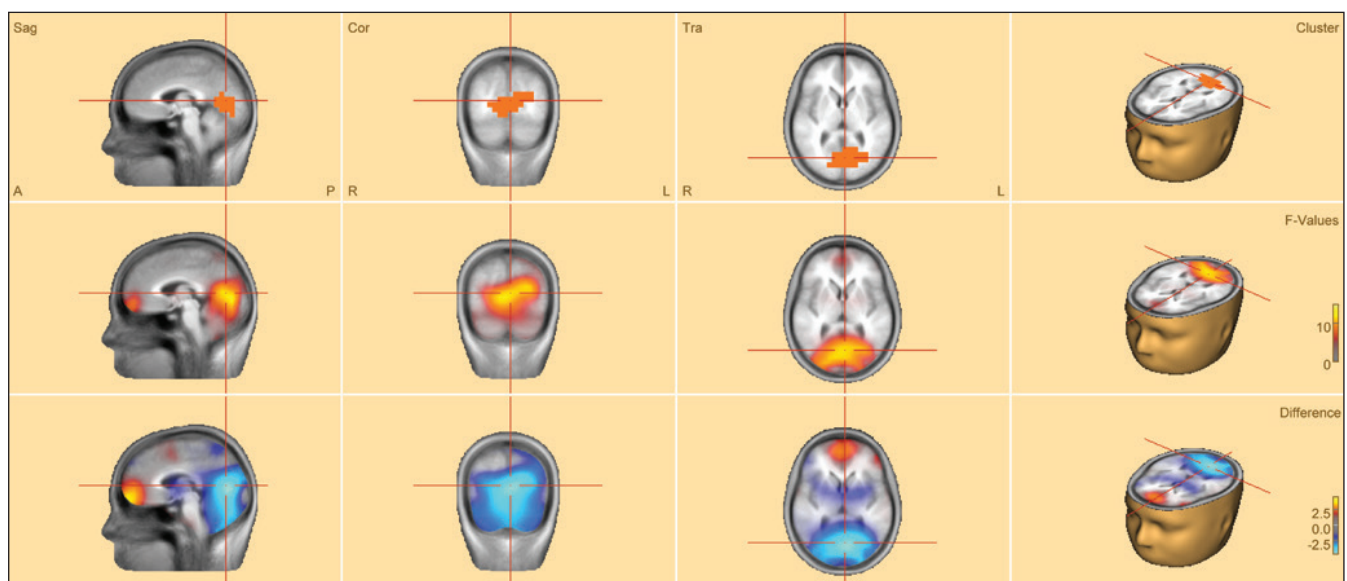


Fig. 4. ANOVA post-hoc analysis: PCC_{ABS} vs. OCC_{ABS} . The first row shows the cluster of significance ($P < 0.05$), the second row shows F-values and the third row shows the percentage difference between source channels.

vided in supplementary materials (Fig. S4 to Fig. S8). As mentioned in section 2.7, the fMRI results required additional verification as we used a non-orthogonal contrast. The analysis performed with the use of randomly assigned ABS vectors did not reveal activations in the abovementioned regions of interest recognized as the DMN (supplementary Fig. S9).

Finally, we directly compared the PCC_{ABS} with OCC_{ABS} conditions using a paired t-test analysis without introducing any other factors to the GLM analysis (Fig. 7, Table SIII, $P < 0.05$ AlphaSim corrected for multiple comparisons, after passing an uncorrected threshold of $P = 0.005$). This analysis showed that PCC_{ABS} was less related with activity within the occipital lobe than OCC_{ABS} , especially in bilateral calcarine fissures, lingual

gyri, occipital gyri, fusiform gyri and cuneus. This outcome was congruent with findings of the beamformer analysis (Fig. 4).

DISCUSSION

The present study revealed two subsystems as possible sources of ABS activity: first, related to the medial prefrontal cortex and precuneus/posterior cingulate gyrus, regions typically reported as nodes of the DMN, and the second, associated with the occipital cortex – a part of the thalamo-cortical circuit. The latter circuit was postulated earlier as a foundation of the alpha rhythm (Ben-Simon et al. 2008, Con-

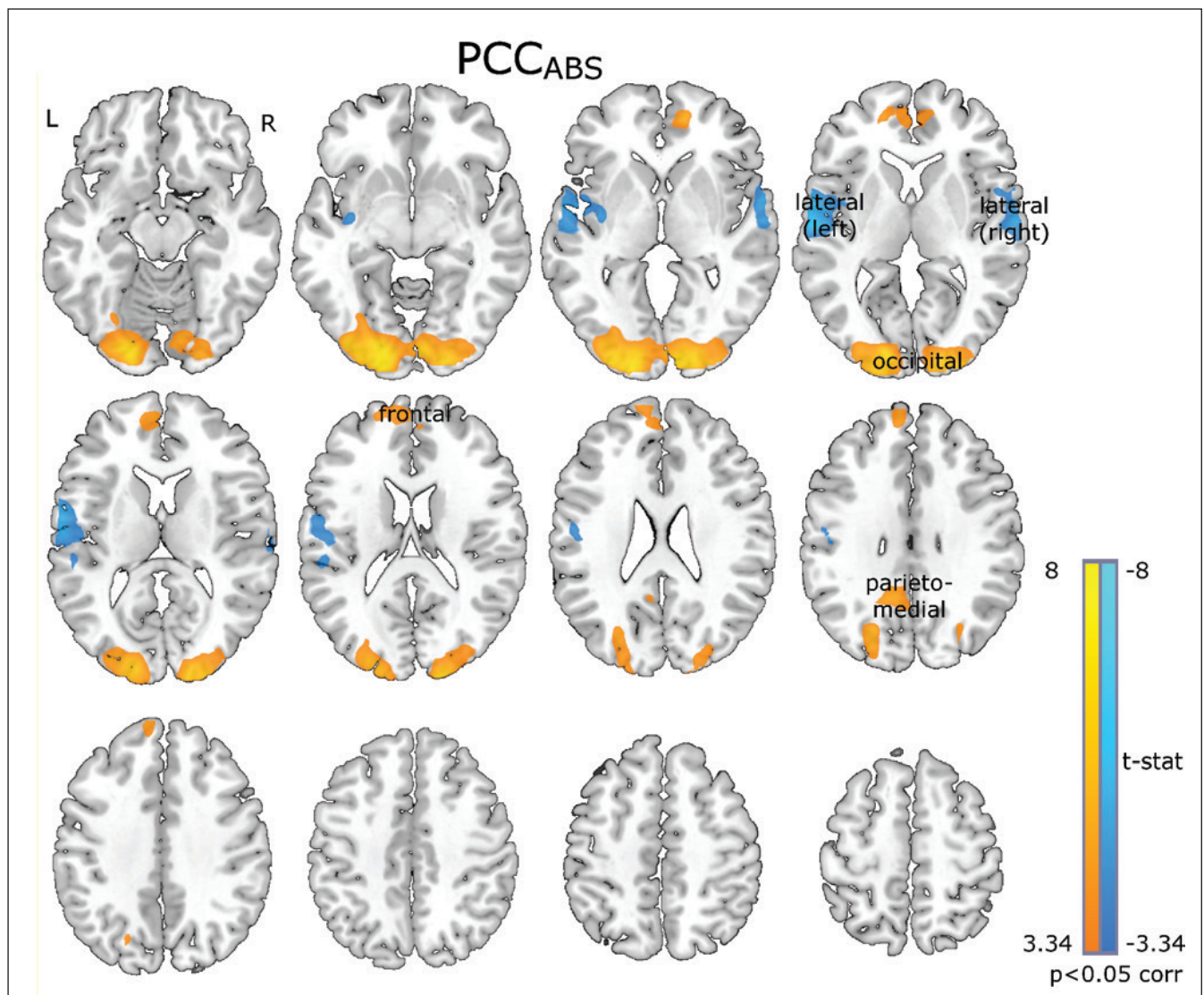


Fig. 5. Group results of the GLM analysis of fMRI data for PCCABS (contrast PCCABS vs. eyes-closed state). The yellow and blue regions represent positive and negative effects respectively. All positive and negative effects were significant after AlphaSim cluster-level correction for multiple comparisons ($P < 0.05$) after passing an uncorrected threshold of $P = 0.001$.

terras and Steriade 1997, DiFrancesco et al. 2008, Feige et al. 2005, Laufs et al. 2003, Lopes da Silva et al. 1973, Lopes Da Silva and Storm Van Leeuwen 1977, Moruzzi and Magoun, 1949, de Munck et al. 2007, Sadaghiani et al. 2010, Steriade et al. 1993). Our results support the concept that the DMN may be an additional or an alternative neuronal correlate of alpha frequency activity, as proposed in several earlier studies (Ben-Simon et al. 2008, Mantini et al. 2007, Mo et al. 2013, Scheeringa et al. 2012). Here we show that the two neural subsystems of alpha activity, although having identical individual alpha frequency differ in (i) temporal distribution of ABS events (Table II, Fig. 2), (ii) their estimated EEG sources (Figs 3 and 4), and (iii) BOLD signal correlates (Figs 5, 6 and 7).

The relationship between ABS activity and the DMN

When we compared the number of the detected events *per* source channel we noted that there were more ABS detected for the DMN than the occipital source channels. The PCC_{ABS} detection rate was smaller than for any other DMN source channel (and still higher than for any of the occipital source channels) but the difference failed to reach significance. Additionally, the detection rate at PCC_{ABS} was not correlated with any other source channel, except for $mPFC_{ABS}$ where the correlation was, however, weak ($r=0.22$). This might be explained either by the fact that the PCC source channel is less related to the ABS origin

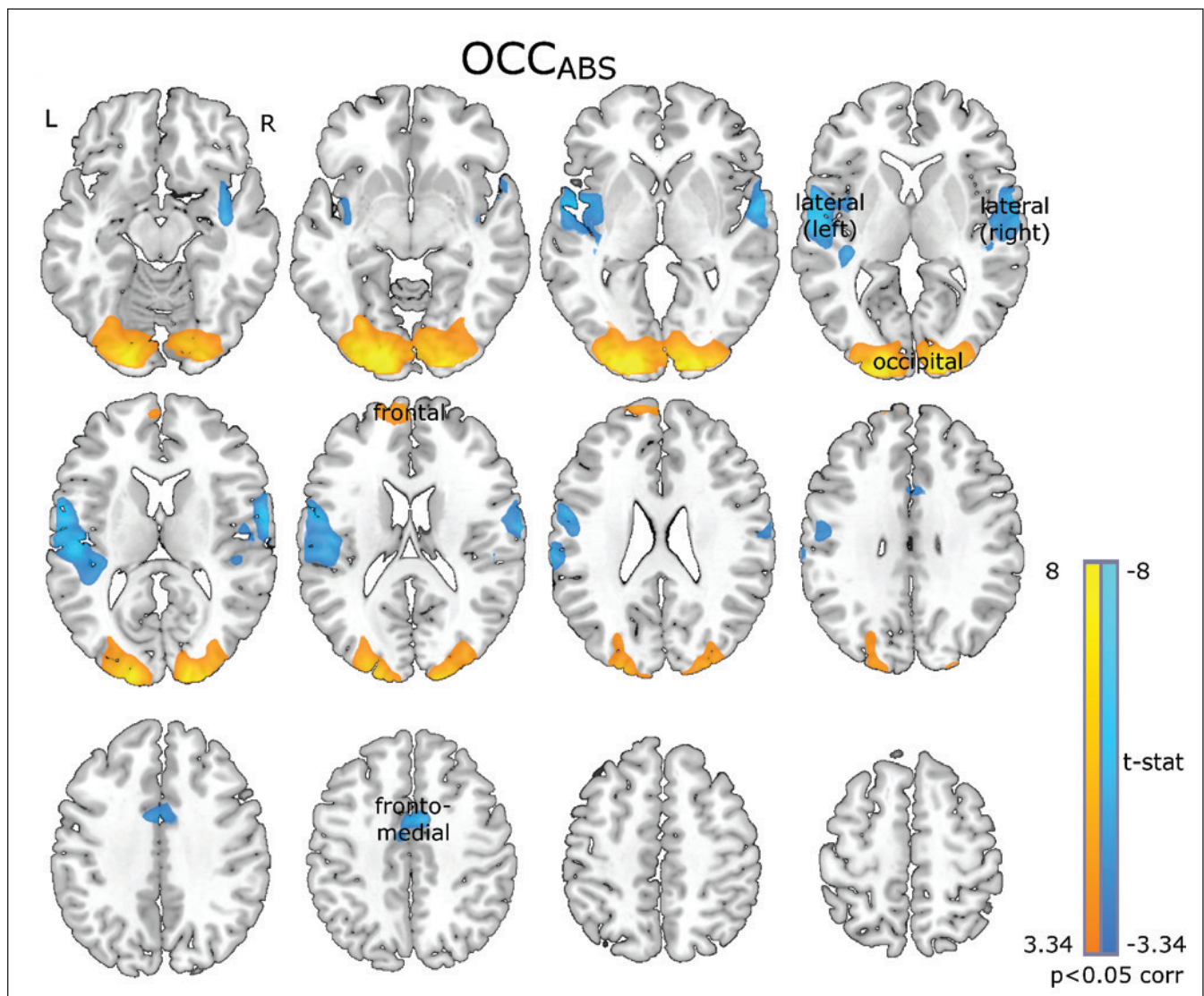


Fig. 6. Group results of the GLM analysis of fMRI data for OCCABS (contrast OCCABS vs. eyes-closed state). The yellow and blue regions represent positive and negative effects, respectively. All positive and negative effects were significant after AlphaSim cluster-level correction for multiple comparisons ($P < 0.05$) after passing an uncorrected threshold of $P = 0.001$.

or that ABS detection performed over this channel is more selective for the activity of DMN (or the potential DMN alpha subsystem) than of any other studied region. The second explanation is supported by many studies indicating that PCC plays a pivotal role in DMN (Fransson and Marrelec 2008, Greicius et al. 2003, Greicius 2008, Raichle et al. 2001). This hypothesis is also reinforced by the fact that the post-hoc analysis of the beamformer source localization indicated the main difference in potential EEG sources between PCC_{ABS} and OCC_{ABS} in occipital lobe. Moreover, the increased BOLD signal change in the parieto-medial cluster was only present when PCC_{ABS} was used as a covariate in the GLM model.

Alpha rhythm and the DMN

A tentative relationship between the resting state alpha rhythm and the DMN has been postulated in previous EEG-fMRI studies (Ben-Simon et al. 2008, Bonnard et al. 2016, Knyazev et al. 2011, Mantini et al. 2007, Mo et al. 2013, Scheeringa et al. 2012). Mantini and colleagues (2007) was the first to indicate that the EEG alpha rhythm may be associated with resting state fMRI networks. The authors correlated six BOLD time courses of resting state networks with waveforms obtained from EEG spectrograms, convolved with the canonical HRF of basic brain rhythms (delta, theta, alpha, beta, and gamma). The recorded alpha rhythm appeared to be positively

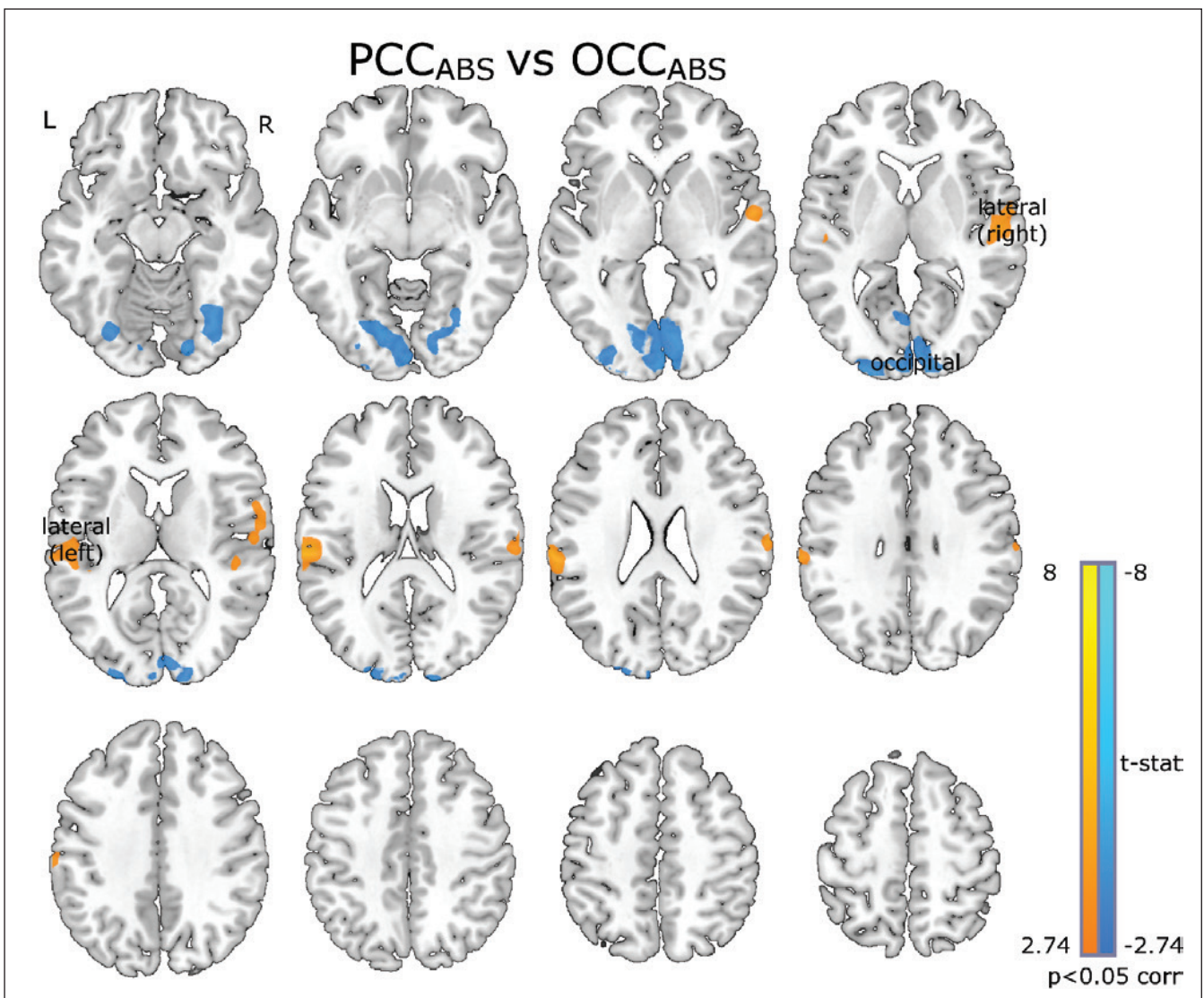


Fig. 7. Group results of the GLM analysis of fMRI data for a paired t-test comparison between PCC_{ABS} and OCC_{ABS} . The yellow and blue regions represent a positive and a negative difference, respectively. They were significant after AlphaSim cluster-level correction for multiple comparisons ($P < 0.05$) after passing an uncorrected threshold of $P = 0.005$.

correlated with activity of the DMN and negatively with BOLD fluctuations in the dorsal attention network and the visual cortex. The DMN activity was also positively correlated with beta band fluctuations, which suggested that the EEG correlates of the DMN are not limited solely to the alpha band. At the same time, Ben-Simon and colleagues (2008) proposed two distinct sources of alpha activity and found that only one of them, called the “spontaneous” subsystem, was correlated with BOLD changes in the DMN. These data were confirmed by the Scheeringa and colleagues (2012), who also reported positive correlation between alpha power and BOLD signal in DMN regions, as well as negative correlation between alpha power and BOLD signal in the occipital cortex.

Mo and colleagues (2013) investigated the relationship between alpha and DMN activity in two separate conditions (eyes-open and eyes-closed) and found positive correlations only for the eyes-open condition. This outcome contradicts the results of the Mantini (2007) who reported a correlation between alpha rhythm and DMN during the eyes-closed condition. This discrepancy might derive from the different analytical approaches; Mo (2013) and Mantini (2007) performed model- and data-driven analyses, respectively. Also, Mo and colleagues (2013) performed alpha rhythm detection selectively over occipital electrodes (O1, O2 and Oz) in a 500 ms short-time Fourier transformation (STFT) window, whereas the Mantini and colleagues (2007) used alpha power calculated from global field power (computed over all channels) in a longer, 1200 ms, STFT window.

The relationship between alpha rhythm and the DMN was also suggested in a TMS experiment, where single pulse stimulation was applied to the mPFC (Bonnard et al. 2016) and compared with stimulation positioned over a hub of the Dorsal Attention Network, the superior parietal lobule (SPL). The study showed that stimulation of the frontal region resulted in higher and longer lasting alpha rhythm synchronization over the occipital lobe than observed following the SPL stimulation. The authors argued that this observation suggested a strong coupling between DMN and occipital alpha rhythm. This interpretation is, however, limited by the fact that the evoked alpha rhythm might have derived from the occipital cortex, medio-parietal brain regions or both.

This short literature review indicates that a relationship between neuronal correlates of alpha rhythm and DMN is plausible. Our study shows that this association can be particularly strong for the PCC_{ABS} activity. However, the computation of particular alpha rhythm differs in the mentioned papers. Ben-Simon and colleagues (2008) introduced a confounding covariate to the GLM representing the eyes-open / eyes-closed conditions. Their procedure separated alpha fluctuations correlated with this paradigm. The remaining alpha rhythm (par-

adigm-independent) was termed “spontaneous alpha rhythm” but the correspondence between the artificially created regressor and the EEG recording was not examined. Scheeringa and colleagues (2012) distinguished the two alpha rhythms (compare Fig. 4 in their work) solely on the basis of a median amplitude criterion, which could fluctuate (Bazanov and Vernon, 2014). Here we showed that the neuronal correlates of PCC_{ABS} are placed in the DMN regions (the medial prefrontal cortex and the precuneus/PCC) and the occipital cortex (Fig. 5). We found also that the occipital cortex was much less related to ABS generation when observed on PCC than on OCC (Fig. 4, Fig. 7) indicating the PCC as more involved in the DMN alpha than the occipital alpha.

Our hypothesis is similar to a postulated relationship between alpha activity, self-referential thinking, and the DMN. In their resting state EEG study Knayazev and colleagues (2011) showed that the alpha band component that was most significantly correlated with self-referential thoughts had a spatial distribution resembling the posterior hub of the DMN encompassing the posterior parietal cortex, occipito-parietal junction, posterior cingulate, and precuneus. Other fMRI studies have also demonstrated that brain networks involved in self-referential thinking resemble the DMN (Gusnard and Raichle 2001, Whitfield-Gabrieli et al. 2011).

Alpha rhythm and the thalamo-occipital circuit

Both applied methods, the beamformer EEG signal analysis and fMRI GLM analysis revealed an occipital cluster as related to the ABS activity (Figs 5 and 6). The regions encompassed by the occipital cluster have been linked to alpha rhythm generation in several previous studies. Schreckenberger and colleagues (2004) used simultaneous EEG-PET imaging to show that increased glucose consumption in the occipital lobes correlated with an increased alpha rhythm amplitude. Furthermore, many EEG-fMRI studies that used both an alternating eyes-open / eyes-closed paradigm (Ben-Simon et al. 2008, 2013, Feige et al. 2005, Liu 2012) and a resting state with eyes-closed experiment (DiFrancesco et al. 2008, Goldman et al. 2002, Laufs et al. 2003, Moosmann et al. 2003, de Munck et al. 2007, Scheeringa et al. 2012, Tyvaert et al. 2008) demonstrated correlations between the occipital BOLD signal and alpha rhythm amplitude.

Basic knowledge derived from intracranial animal studies (Contreras and Steriade 1997, Lopes da Silva et al. 1973, Lopes Da Silva and Storm Van Leeuwen, 1977, Moruzzi and Magoun, 1949 Steriade et al. 1993) established the hypothesis that the alpha rhythm is elicited in the visual (occipital) cortex and the visual thalamus during resting state. This phenomenon could mirror

the relationship between alpha rhythm generated in the thalamo-occipital circuitry and hemodynamic activity, as a reflection of parallel metabolic changes in human studies. Our analysis of fMRI data did not reveal any group-averaged ABS activity in the thalamus (for no source channel). In this respect it is worth mentioning that De Munck and colleagues (2007) demonstrated that the HRF in the thalamus is different to cortical HRF; thus, distinct fMRI modeling should be applied for both regions. We used such an approach in our previous work (Rusiniak et al. 2015) and found considerable inter-subject variability in terms of the ABS activity in the thalamus. We cannot exclude the possibility that the thalamus may be involved in the generation of both “types” of alpha rhythms; it is possible that the ABS-based BOLD regressor could not detect the complex thalamus activity. Moreover, we could not perform ABS detection for any potential thalamus source channel since deep brain structures are not monitorable by the EEG technique. Relatedly, Scheeringa and colleagues (2012) showed that the high and low power alpha differ, with only the latter demonstrating strong functional connectivity between the thalamus and the visual cortex.

The interpretation of fMRI contrast which compared eyes-closed condition with ABS vectors for PCC (Fig.5) and OCC (Fig.6) should be taken with caution especially in terms of the sign of correlation. The occipital cluster activation revealed by the GLM analysis using ABS vectors for PCC and OCC was influenced by both: paradigm timing and ABS regressor. The change of BOLD signal in occipital cluster may result from outflow of oxygenated blood due to lack of visual stimulation and/or increased alpha activity (Fig. S10). The fMRI contrast (ABS vs. eyes-closed) indicated that the BOLD signal was higher during ABS than during eyes-closed periods in regions marked by positive values (Figs 5 and 6). This positive sign, however, did not imply that ABS related brain activity was reflected by BOLD signal increase in a given region, and it was not aimed by this analysis. The above concern does not apply to direct comparison of PCC_{ABS} and OCC_{ABS} (Fig. 7), which indicated that [activation of] occipital cortex was less related to ABS in PCC than in OCC.

Interestingly, the beamformer analysis (Figs 3 and 4) although not contaminated by visual input during eyes-open did indicate that PCC_{ABS} and OCC_{ABS} were related to sources located in the occipital cluster. Note, however, that in line with fMRI results beamformer revealed that parieto-medial region was only active for ABS detected using PCC source channel (PCC_{ABS} ; cluster of significance indicated in top row of Fig. 4). The presented discrepancy in brain active regions between PCC_{ABS} and OCC_{ABS} fMRI indicated results (Fig. 7) and beamformer re-

sults (Fig. 4) suggest two different mechanisms of elicitation of alpha rhythm.

Two components of the resting state alpha rhythm: DMN alpha and occipital alpha

We posit that the resting state alpha rhythm (Berger rhythm) consists of two different but co-occurring phenomena: the occipital alpha rhythm supported by the thalamo-occipital circuit and the DMN alpha related to the activity in brain regions typically described as the DMN hubs. We furthermore argue that there is a relationship between the DMN alpha activity driven by PCC_{ABS} and the “spontaneous alpha rhythm” described by Ben-Simon and colleagues (2008) or “high (power) alpha,” as termed by the Scheeringa and colleagues (2012). In both these works the selected alpha rhythm correlated with activity in the medial prefrontal cortices and precuneus, which matched our EEG results (Fig. 4) and fMRI data (Fig. 5). At the same time, we propose that the occipital alpha driven by OCC_{ABS} reflects the “induced alpha rhythm” (Ben-Simon et al. 2008) or the “low-amplitude alpha” activity (Scheeringa et al. 2012). This type of alpha rhythm has a clear source in the occipital area and probably reflects oscillations identified in many other studies as the alpha rhythm associated with the thalamo-occipital circuit (Contreras and Steriade 1997, DiFrancesco et al. 2008, Feige et al. 2005, Goldman et al. 2002, Lopes da Silva et al. 1973, Lopes Da Silva and Storm Van Leeuwen 1977, Moosmann et al. 2003, Moruzzi and Magoun, 1949, de Munck et al. 2007, Sadaghiani et al. 2010, Steriade et al. 1993). One potential reason why the regions found here as related to the DMN alpha (the parieto-medial and frontal cluster) have not been observed in previous works, is that the DMN alpha is of much smaller power than the occipital alpha rhythm (Fig. 4) and partially co-exists with the latter in the spatio-temporal domain. This might be the reason why the typical FFT or STFT approaches, used in a number of studies (quoted in this manuscript), have failed to differentiate these phenomena. Applying ABS detection over source channel montage allows to separate these two alpha modes and the underlying neural systems.

The ABS detection algorithm

The two most common approaches to the analysis of temporal changes of continuous EEG signals in the literature are STFT (Allen 1977) and microstates classification (Britz et al. 2010, Musso et al. 2010). Both have been used for alpha rhythm investigation with simultaneous

EEG-fMRI registration (Mantini et al. 2007, Musso et al. 2010, Liu 2012) but both have also serious shortcomings to be used for ABS detection.

The STFT is commonly computed on short (1–2 s) consecutive periods of the signal and therefore considerably reduces temporal resolution of EEG. In general, this resolution is still sufficient with respect to the temporal resolution of fMRI. As ABS can occur within extremely short intervals the precise determination of their onsets and the interval between them impact the final shape of the predicted response during fMRI analysis (Miezin et al. 2000) and EEG source localization. The increased alpha frequency power was observed solely during the eyes-closed condition similarly: within single subject and at the group level (Fig. S10). The fMRI analysis did not allow to differentiate spontaneous brain activity related to alpha rhythm generation from activity induced by visual input because of its limited temporal resolution (~2s). In this work we present a new analytical approach based on individual alpha burst waveform and performed in time domain that allows to investigate dynamics of ABS activity with a millisecond precision. STFT cannot, however, differentiate possible brain subsystems related to alpha activity as they can share the same frequency. Such differentiation can be addressed by considering other aspects of alpha rhythm, including the spindle-form segmental organization (Bazanov and Vernon 2014, Timofeev et al. 2002) which can independently detect ABS activity.

In comparison to STFT, the microstates analysis provides much better temporal resolution (~150 ms) but in is mainly focused on the spatial distribution of the signal in the form of quasi-stable spectral scalp distributions (“classes”). Although the Berger effect is well-described in terms of scalp distribution, its identification without the frequency characteristic might provide biased results.

We developed an ABS detection algorithm in order to overcome the aforementioned limitations. Following recent publications (Bazanov and Vernon 2014, Ben-Simon et al. 2013), we propose that an ABS-based approach alongside FFT analysis might provide additional information on the Berger effect.

General methodological remarks

A significant advantage of our study is the large ($n=36$) and homogenous (young males) subject pool. This group was selected due to previous reports demonstrating significant sex and age differences with respect to alpha rhythm parameters (Chiang et al. 2011). At the same time, we acknowledge that the homogeneity of our

experimental group implies that the conclusions cannot be extrapolated to the general population.

In keeping with other research (Ben-Simon et al. 2008, 2013, Feige et al. 2005 Liu 2012), we decided to use a block paradigm with subjects alternately closing and opening their eyes (the classical “Berger experiment”). Other researchers have used the eyes-closed condition across the entire EEG session (a “resting state experiment” (DiFrancesco et al. 2008, Goldman et al. 2002, Laufs et al. 2003, Mantini et al. 2007, Moosmann et al. 2003, de Munck et al. 2007, Mantini et al. 2007, Scheeringa et al. 2012, Tyvaert et al. 2008). The latter paradigm prevents BOLD signal variation due to visual stimulation but precludes comparisons of the results with experiments searching for neuronal mechanisms underlying the Berger effect. The Berger rhythm has traditionally been recorded during eyes-closed states, whereas the DMN has been measured in fMRI experiments in both eyes-closed and eyes-open conditions (Zou et al. 2009). Only minor differences have been shown between the latter two conditions, probably due to the fact that no visual stimulation was used and participants were looking at a black screen in MRI goggles (Greicius et al. 2003). We observed both ABS and brain activity resembling DMN activity during eyes-open and eyes-closed states but they were significantly more pronounced in the eyes-closed condition (Fig. 2, Fig. 7). It is worth noting that the DMN can co-exist with simple tasks (e.g. eyes-closed / eyes-open) as has been proved by the Fair (2007) and Greicius (2003).

Our EEG analysis revealed LAG_{ABS} and RAG_{ABS} as having the highest detection rate from among all the analysed source channels. Nevertheless, our fMRI results showed no activity around these regions. These regions have been proposed as only additional (Raichle et al. 2001) or non-essential DMN nodes (Allen et al. 2011). We believe that the potential reason for detecting alpha activity in angular gyri is that the ABS detection algorithm performed over these source channels detected common events related to both the DMN alpha and the occipital alpha. This assumption was partially confirmed by the additional post-hoc analysis of the beamformer outcomes showing that the PCC_{ABS} differs significantly from LAG_{ABS} and RAG_{ABS} only in the left-hemisphere occipital cortex (although the size of the significant cluster was very small) (Fig. S2 and Fig. S3).

Furthermore, using the $MPFC_{ABS}$ as a GLM regressor provided very similar outcomes when compared to the OCC_{ABS} (Fig. 6), LAG_{ABS} (Fig. S5), the RAG_{ABS} (Fig. S6) and the PCC_{ABS} regressors. The frontal cluster was present in all the results, but the activation was most sizeable when based on the PCC_{ABS} (Table SI and Table SII). Therefore, we are unable to unambiguously assign the revealed frontal cluster to only one alpha rhythm (occipital or

DMN). However, due to the fact that frontal cluster is present in all fMRI results (Figs 5, 6 and Figs S4–S8) and the PCC_{ABS} was found weakly correlated with mPFC_{ABS} (Table II) but not correlated with any other results we suggest that the frontal cluster is related mainly to the DMN alpha subsystem. In addition, results of a number of other experiments (i.e., Greicius, 2008, Raichle et al. 2001) have indicated strong connections between the parieto-medial and the frontal clusters.

To conclude we posit that the resting state alpha rhythm should be considered as a complex activity consisting of two components: the occipital alpha rhythm and the more subtle DMN alpha rhythm. In conjunction with existing physiological data, our results suggest that the neuronal correlates of the DMN alpha rhythm might be located in two main nodes of DMN: the medio-parietal (PCC and precuneus) and the frontal (mPFC), whereas the occipital alpha rhythm in the thalamo-occipital circuit.

Abbreviations used

ABS – alpha bursting segments
LAG – left anterior gyrus
LOCC – left occipital cortex
mPFC – medial prefrontal cortex
OCC – bilateral occipital cortex
PCC – posterior cingulate cortex
RAG – right anterior gyrus
ROCC – right occipital cortex
STFT – short-time Fourier transformation

Data availability

The data supporting major findings of this study are available from the corresponding author upon a reasonable request.

ACKNOWLEDGMENTS

This study was supported by a grant from the Polish National Science Center no. 2011/01/N/NZ4/04985.

AUTHORS' CONTRIBUTION

MR and TW designed the experiment and paradigm. MR and ML collected the data. MR and TW analyzed the data. MR designed and prepared the figures.

All authors reviewed and discussed the results. MR, KC, AW, AP and TW wrote the manuscript.

REFERENCES

- Allen EA, Erhardt EB, Damaraju E, Gruner W, Segall JM, Silva RF, Havlicek M, Rachakonda S, Fries J, Kalyanam R, Michael AM, Caprihan A et al. (2011) A Baseline for the Multivariate Comparison of Resting-State Networks. *Front Syst Neurosci* 5: 2.
- Allen JB (1977) Short term spectral analysis, synthesis, and modification by discrete Fourier transform. *IEEE Trans Acoust Speech Signal Process* 25: 235–238.
- Allen PJ, Josephs O, Turner R (2000) A Method for Removing Imaging Artifact from Continuous EEG Recorded during Functional MRI. *NeuroImage* 12: 230–239.
- Angelakis E, Lubar JF, Stathopoulou S (2004) Electroencephalographic peak alpha frequency correlates of cognitive traits. *Neurosci Lett* 371: 60–63.
- Anokhin A, Steinlein O, Fischer C, Mao Y, Vogt P, Schall E, Vogel F (1992) A genetic study of the human low-voltage electroencephalogram. *Hum Genet* 90: 99–112.
- Başar E, Schürmann M, Başar-Eroglu C, Karakaş S (1997) Alpha oscillations in brain functioning: an integrative theory. *Int J Psychophysiol Off J Int Organ Psychophysiol* 26: 5–29.
- Bazanava OM, Vernon D (2014) Interpreting EEG alpha activity. *Neurosci Biobehav Rev* 44: 94–110.
- Ben-Simon E, Podlipsky I, Arieli A, Zhdanov A, Hendler T (2008) Never resting brain: Simultaneous representation of two alpha related processes in humans. *PLoS ONE* 3: e3984.
- Ben-Simon E, Podlipsky I, Okon-Singer H, Gruberger M, Cvetkovic D, Intrator N, Hendler T (2013) The dark side of the alpha rhythm: fMRI evidence for induced alpha modulation during complete darkness. *Eur J Neurosci* 37: 795–803.
- Berger PDH (1929) Über das Elektrenkephalogramm des Menschen. *Arch Für Psychiatr Nervenkrankh* 87: 527–570.
- Bishop GH (1936) The Interpretation of Cortical Potentials. *Cold Spring Harb Symp Quant Biol* 4: 305–319.
- Bonnard M, Chen S, Gaychet J, Carrere M, Woodman M, Giusiano B, Jirsa V (2016) Resting state brain dynamics and its transients: a combined TMS-EEG study. *Sci Rep* 6: 31220.
- Britz J, Van De Ville D, Michel CM (2010) BOLD correlates of EEG topography reveal rapid resting-state network dynamics. *NeuroImage* 52: 1162–1170.
- Chiang AKI, Rennie CJ, Robinson PA, Albada SJ van, Kerr CC (2011) Age trends and sex differences of alpha rhythms including split alpha peaks. *Clin Neurophysiol* 122: 1505–1517.
- Cole SR, Voytek B (2017) Brain Oscillations and the Importance of Waveform Shape. *Trends Cogn Sci* 21: 137–149.
- Contreras D, Steriade M (1997) Synchronization of low-frequency rhythms in corticothalamic networks. *Neuroscience* 76: 11–24.
- Debener S, Mullinger KJ, Niazy RK, Bowtell RW (2008) Properties of the ballistocardiogram artefact as revealed by EEG recordings at 1.5, 3 and 7 T static magnetic field strength. *Int J Psychophysiol* 67: 189–199.
- DiFrancesco MW, Holland SK, Szaflarski JP (2008) Simultaneous EEG/Functional Magnetic Resonance Imaging at 4 Tesla: Correlates of Brain Activity to Spontaneous Alpha Rhythm During Relaxation. *J Clin Neurophysiol Off Publ Am Electroencephalogr Soc* 25: 255–264.
- Fair DA, Schlaggar BL, Cohen AL, Miezin FM, Dosenbach NUF, Wenger KK, Fox MD, Snyder AZ, Raichle ME, Petersen SE (2007) A method for using blocked and event-related fMRI data to study “resting state” functional connectivity. *NeuroImage* 35: 396–405.
- Feige B, Scheffler K, Esposito F, Salle FD, Hennig J, Seifritz E (2005) Cortical and Subcortical Correlates of Electroencephalographic Alpha Rhythm Modulation. *J Neurophysiol* 93: 2864–2872.
- Fransson P, Marrelec G (2008) The precuneus/posterior cingulate cortex plays a pivotal role in the default mode network: Evidence from a partial correlation network analysis. *NeuroImage* 42: 1178–1184.

- Garcia D (2010) Robust smoothing of gridded data in one and higher dimensions with missing values. *Comput Stat Data Anal* 54: 1167–1178.
- Goldman RI, Stern JM, Engel J, Cohen MS (2002) Simultaneous EEG and fMRI of the alpha rhythm. *Neuroreport* 13: 2487–2492.
- Greicius M (2008) Resting-state functional connectivity in neuropsychiatric disorders. *Curr Opin Neurol* 21: 424–430.
- Greicius MD, Krasnow B, Reiss AL, Menon V (2003) Functional connectivity in the resting brain: A network analysis of the default mode hypothesis. *Proc Natl Acad Sci* 100: 253–258.
- Gross J, Kujala J, Hämäläinen M, Timmermann L, Schnitzler A, Salmelin R (2001) Dynamic imaging of coherent sources: studying neural interactions in the human brain. *Proc Natl Acad Sci* 98: 694–699.
- Gusnard DA, Raichle ME (2001) Searching for a baseline: Functional imaging and the resting human brain. *Nat Rev Neurosci* 2: 685–694.
- Ille N, Berg P, Scherg M (2002) Artifact correction of the ongoing EEG using spatial filters based on artifact and brain signal topographies. *J Clin Neurophysiol Off Publ Am Electroencephalogr Soc* 19: 113–124.
- Klimesch W, Schimke H, Pfurtscheller G (1993) Alpha frequency, cognitive load and memory performance. *Brain Topogr* 5: 241–251.
- Knyazev GG, Slobodskoj-Plusnin JY, Bocharov AV, Pyrkova LV (2011) The default mode network and EEG alpha oscillations: An independent component analysis. *Brain Res* 1402: 67–79.
- Lansky P, Bohdanecký Z, Indra M, Radil-Weiss T (1979) Alpha detection: some comments on Hardt and Kamiya, “Conflicting results in EEG alpha feedback studies.” *Biofeedback Self-Regul* 4: 127–131.
- Laufs H, Holt JL, Elfont R, Krams M, Paul JS, Krakow K, Kleinschmidt A (2006) Where the BOLD signal goes when alpha EEG leaves. *NeuroImage* 31: 1408–1418.
- Laufs H, Kleinschmidt A, Beyerle A, Eger E, Salek-Haddadi A, Preibisch C, Krakow K (2003) EEG-correlated fMRI of human alpha activity. *NeuroImage* 19: 1463–1476.
- Liu TT (2012) The development of event-related fMRI designs. *NeuroImage* 62: 1157–1162.
- Livanov MN (1984) Rhythms of the electroencephalogram and their functional significance. *Zhurnal Vyssheĭ Nervn Deiatelnosti Im P Pavlova* 34: 613–626.
- Lopes da Silva FH, Lierop TH van, Schrijer CF, Leeuwen WS van (1973) Organization of thalamic and cortical alpha rhythms: spectra and coherences. *Electroencephalogr Clin Neurophysiol* 35: 627–639.
- Lopes Da Silva FH, Storm Van Leeuwen W (1977) The cortical source of the alpha rhythm. *Neurosci Lett* 6: 237–241.
- Mantini D, Perrucci MG, Del Gratta C, Romani GL, Corbetta M (2007) Electrophysiological signatures of resting state networks in the human brain. *Proc Natl Acad Sci* 104: 13170–13175.
- Miezin FM, Maccotta L, Ollinger JM, Petersen SE, Buckner RL (2000) Characterizing the Hemodynamic Response: Effects of Presentation Rate, Sampling Procedure, and the Possibility of Ordering Brain Activity Based on Relative Timing. *NeuroImage* 11: 735–759.
- Mo J, Liu Y, Huang H, Ding M (2013) Coupling between visual alpha oscillations and default mode activity. *NeuroImage* 68: 112–118.
- Moosmann M, Ritter P, Krastel I, Brink A, Thees S, Blankenburg F, Taskin B, Obrig H, Villringer A (2003) Correlates of alpha rhythm in functional magnetic resonance imaging and near infrared spectroscopy. *NeuroImage* 20: 145–158.
- Moruzzi G, Magoun HW (1949) Brain stem reticular formation and activation of the EEG. *Electroencephalogr Clin Neurophysiol* 1: 455–473.
- Munck JC de, Gonçalves SI, Huijboom L, Kuijper JPA, Pouwels PJW, Heethaar RM, Lopes da Silva FH (2007) The hemodynamic response of the alpha rhythm: An EEG/fMRI study. *NeuroImage* 35: 1142–1151.
- Musso F, Brinkmeyer J, Mobascher A, Warbrick T, Winterer G (2010) Spontaneous brain activity and EEG microstates. A novel EEG/fMRI analysis approach to explore resting-state networks. *NeuroImage* 52: 1149–1161.
- Niedermeyer E (2005) The normal EEG of the waking adult. *Electroencephalogr Basic Princ Clin Appl Relat Fields* pp. 149–173.
- Oldfield RC (1971) The assessment and analysis of handedness: the Edinburgh inventory. *Neuropsychologia* 9: 97–113.
- Raichle ME, MacLeod AM, Snyder AZ, Powers WJ, Gusnard DA, Shulman GL (2001) A default mode of brain function. *Proc Natl Acad Sci* 98: 676–682.
- Rusiniak M, Lewandowska M, Wolak T, Pluta A, Milner R, Ganc M, Włodarczyk A, Senderski A, Śliwa L, Skarżyński H (2013) A modified oddball paradigm for investigation of neural correlates of attention: a simultaneous ERP-fMRI study. *Magn Reson Mater Phys Biol Med* 26: 511–526.
- Rusiniak M, Lewandowska M, Wolak T, Milner R, Cieśla K, Pluta A, Skarzynski H (2014) Verification of alpha rhythm hemispherical dominance using simultaneous EEG-fMRI registration. In: *Organization for Human Brain Mapping, Hamburg, Germany, poster 4204*.
- Rusiniak M, Lewandowska M, Pluta A, Cieśla K, Wojcik J, Wolak T (2015) Intersubject variability of thalamic activation during generation of Berger’s alpha rhythm. *J Hear Sci* 5: 16–22.
- Sadaghiani S, Scheeringa R, Lehongre K, Morillon B, Giraud A-L, Kleinschmidt A (2010) Intrinsic Connectivity Networks, Alpha Oscillations, and Tonic Alertness: A Simultaneous Electroencephalography/Functional Magnetic Resonance Imaging Study. *J Neurosci* 30: 10243–10250.
- Scheeringa R, Petersson KM, Kleinschmidt A, Jensen O, Bastiaansen MCM (2012) EEG Alpha Power Modulation of fMRI Resting-State Connectivity. *Brain Connect* 2: 254–264.
- Schreckenberger M, Lange-Asschenfeld C, Lochmann M, Mann K, Siessmeier T, Buchholz H-G, Bartenstein P, Gründer G (2004) The thalamus as the generator and modulator of EEG alpha rhythm: a combined PET/EEG study with lorazepam challenge in humans. *NeuroImage* 22: 637–644.
- Schürmann M, Demiralp T, Başar E, Başar Eroglu C (2000) Electroencephalogram alpha (8-15 Hz) responses to visual stimuli in cat cortex, thalamus, and hippocampus: a distributed alpha network? *Neurosci Lett* 292: 175–178.
- Steriade M, McCormick DA, Sejnowski TJ (1993) Thalamocortical oscillations in the sleeping and aroused brain. *Science* 262: 679–685.
- Timofeev I, Grenier F, Bazhenov M, Houweling AR, Sejnowski TJ, Steriade M (2002) Short- and medium-term plasticity associated with augmenting responses in cortical slabs and spindles in intact cortex of cats in vivo. *J Physiol* 542: 583–598.
- Timofeev I, Bazhenov M (2005) Mechanisms and biological role of thalamocortical oscillations. *Trends Chronobiol Res* pp. 1–47.
- Tyvaert L, LeVan P, Grova C, Dubeau F, Gotman J (2008) Effects of fluctuating physiological rhythms during prolonged EEG-fMRI studies. *Clin Neurophysiol* 119: 2762–2774.
- Whitfield-Gabrieli S, Moran JM, Nieto-Castañón A, Triantafyllou C, Saxe R, Gabrieli JDE (2011) Associations and dissociations between default and self-reference networks in the human brain. *NeuroImage* 55: 225–232.
- Zhan Z, Xu L, Zuo T, Xie D, Zhang J, Yao L, Wu X (2014) The contribution of different frequency bands of fMRI data to the correlation with EEG alpha rhythm. *Brain Res* 1543: 235–243.
- Zou Q, Long X, Zuo X, Yan C, Zhu C, Yang Y, Liu D, He Y, Zang Y (2009) Functional connectivity between the thalamus and visual cortex under eyes closed and eyes open conditions: A resting-state fMRI study. *Hum Brain Mapp* 30: 3066–3078.

Supplementary material

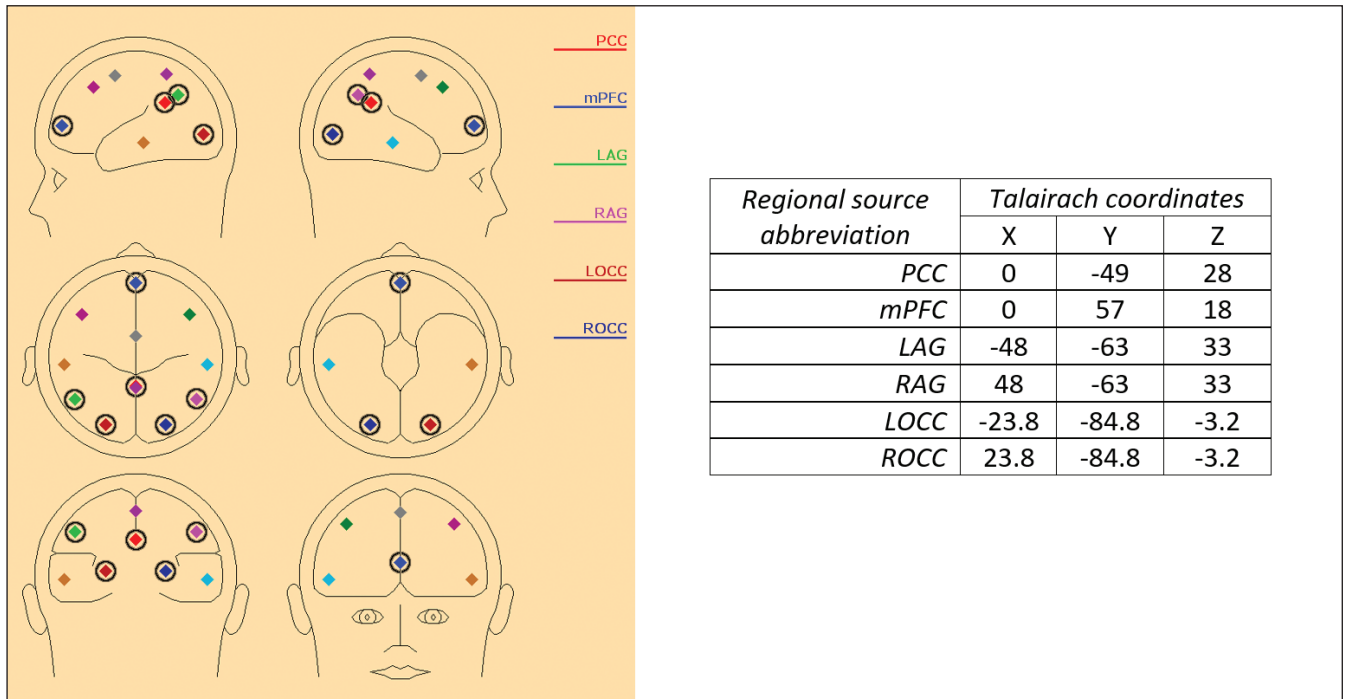


Fig. S1. EEG Montage of Default Mode Network with Noise Sources. The source channel positions are represented by color diamonds. The source channels used for ABS computation are indicated by black circles; the Talairach coordinates are shown in the adjacent table.

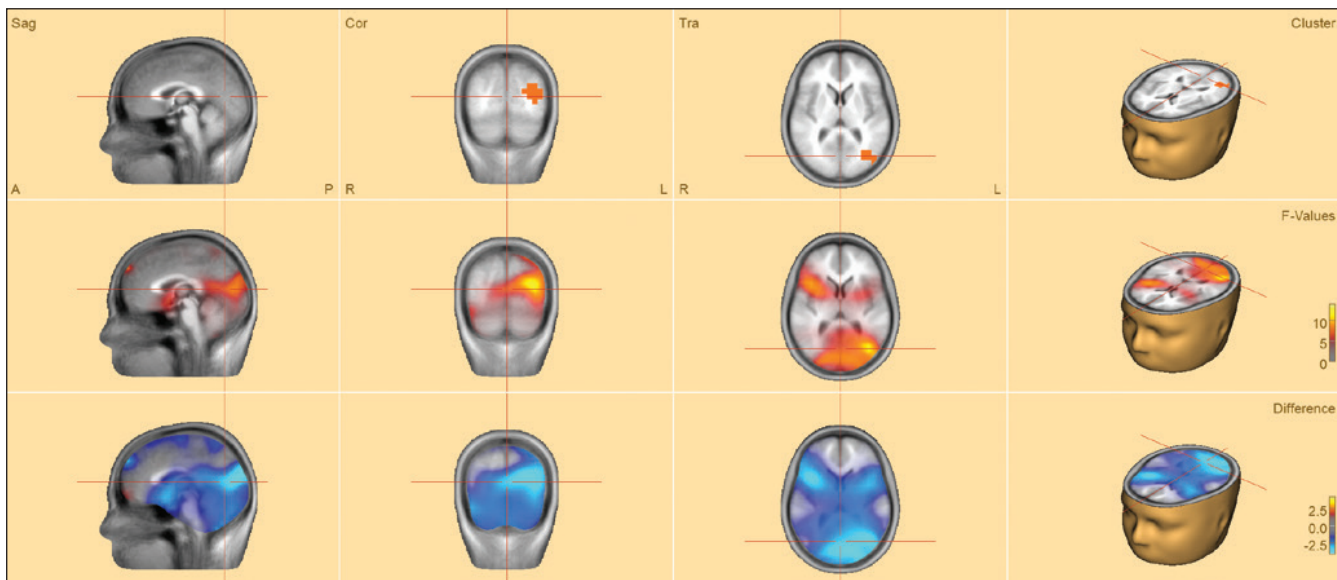


Fig. S2. ANOVA Post-hoc analysis: PCC_{ABS} vs. LAG_{ABS} . The first row shows the cluster of significance ($P < 0.05$), the second row shows F-values and the third row the percentage difference between source channels.

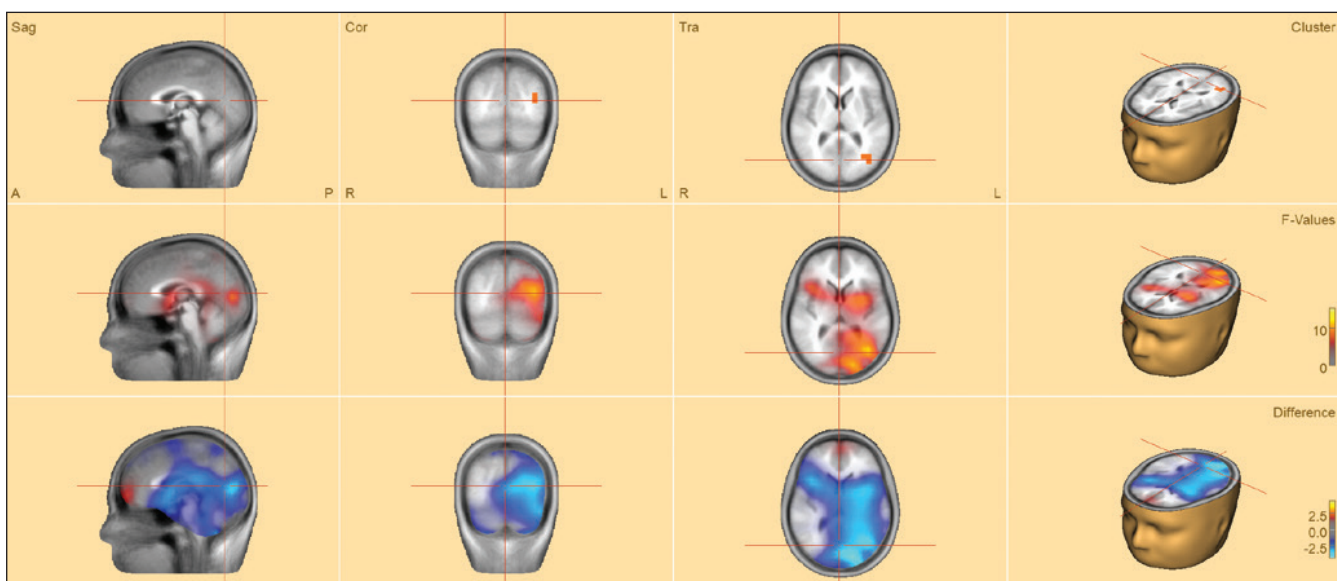


Fig. S3. ANOVA post-hoc analysis: PCC_{ABS} vs. RAG_{ABS} . The first row shows the cluster of significance ($P < 0.05$), the second row shows F-values and the third row the percentage difference between source channels.

Table S1. fMRI results for PCC_{ABS} (as shown in Fig. 5).

	Cluster	Cluster size [cm ³]	Main AAL* region	Talairach coordinates			Max t-value	Area size [cm ³]	
				X	Y	Z			
positive t-values	frontal	6.40	left superior frontal gyrus	-12	40	45	4.3	4.65	
			right superior frontal gyrus	15	47	-2	4.6	1.16	
	parieto-medial	1.50	cingulate gyrus, posterior	-9	-49	32	4.4	0.53	
			precuneus	-10	-50	31	4.4	0.70	
	occipital	43.31	left calcarine fissure	-18	-96	1	7.0	3.20	
			right calcarine fissure	12	-92	4	6.4	2.94	
			cuneus	16	-95	19	6.2	1.42	
			left lingual gyrus	-18	-85	-3	6.9	2.92	
			right lingual gyrus	8	-88	0	6.2	3.60	
			left occipital gyrus	-18	-94	-1	7.1	17.14	
			right occipital gyrus	18	-95	20	6.2	4.90	
			left fusiform gyrus	-20	-85	-3	6.9	1.06	
			right fusiform gyrus	27	-84	3	4.4	0.45	
			negative t-values	lateral	left	10.33	left rolandic operculum	-57	-1
left postcentral gyrus	-59	-9					13	-4.5	2.07
left insula	-46	-5					-1	-4.3	0.90
left temporal gyrus	-62	-10					7	-5.6	3.78
right	3.06	right rolandic operculum		-61	5	4	-4.5	0.68	
		right temporal gyrus		61	1	1	-5.1	2.18	

* The merged Automated Anatomical Labeling was used, as introduced by PMOD (<http://doc.pmod.com/pneuro/6750.htm>), with additional small structures joined (as compared to MNI-AAL in: Tzourio-Mazoyer et al., 2002). Medial structures, including the cingulate gyrus, precuneus and cuneus were presented regardless of hemisphere.

Table SII. fMRI results for OCC_{ABS} (as shown in Fig. 6).

	Cluster	Cluster size [cm ³]	Main AAL* region	Talairach coordinates			Max z-score	Area size [cm ³]	
				X	Y	Z			
positive t-values	occipital	56.43	left calcarine fissure	-18	-94	2	9.9	4.86	
			right calcarine fissure	18	-92	9	8.7	3.84	
			cuneus	16	-94	11	8.3	1.57	
			left lingual gyrus	-15	-89	4	8.3	4.17	
			right lingual gyrus	20	-94	-1	7.7	5.09	
			left occipital gyrus	-18	-93	3	9.9	18.19	
			right occipital gyrus	19	-92	10	8.7	10.28	
			left fusiform gyrus	-18	-85	-2	7.3	2.15	
			right fusiform gyrus	26	-84	-6	5.7	1.39	
			cerebellum	22	-85	-12	6.2	2.14	
	frontal	3.26	left superior frontal gyrus	-14	62	16	4.9	3.20	
	fronto-medial	2.60	cingulate gyrus, middle part	4	3	38	5.8	2.26	
negative t-values	lateral	left	21.69	left rolandic operculum	-55	-2	7	6.4	4.14
				left precentral gyrus	-54	1	19	5.7	1.24
				left postcentral gyrus	-51	-19	16	5.8	4.01
				left insula	-46	3	-3	4.9	2.04
				left temporal gyrus	-53	-7	5	6.5	6.39
		right	1.34	right Rolandic operculum	61	0	10	6.1	2.80
		right postcentral gyrus		65	-8	14	5.9	1.50	
		right temporal gyrus		61	-1	3	5.9	3.70	
		right Heshl gyrus		61	-1	6	5.7	0.70	

* The merged Automated Anatomical Labeling was used, as introduced by PMOD (<http://doc.pmod.com/pneuro/6750.htm>), with additional small structures joined (as compared to MNI-AAL in: Tzourio-Mazoyer et al., 2002). Medial structures, including the cingulate gyrus, precuneus and cuneus were presented regardless of hemisphere.

Table SIII. Paired t-test fMRI analysis of PCC_{ABS} vs. OCC_{ABS} (as shown in Fig. 7).

	Cluster	Cluster size [cm ³]	Main AAL* region	Talairach coordinates			Max z-score	Area size [cm ³]	
				X	Y	Z			
positive t-values	lateral	left 4.41	left postcentral gyrus	-53	0	18	4.3	1.00	
			left temporal gyrus	-63	-23	17	4.6	1.36	
			left supramarginal gyrus	-64	-21	19	4.7	1.85	
		right 4.36	right Rolandic operculum	61	-2	8	3.7	1.05	
			right supramarginal gyrus	65	-15	22	4.1	0.97	
			right temporal gyrus	53	-14	7	4.0	1.79	
				right Heschl gyrus	51	-13	8	3.7	0.54
	negative t-values	occipital	22.92	left calcarine fissure	2	-94	1	3.6	3.96
right calcarine fissure				9	-63	6	3.4	2.06	
cuneus				16	-95	19	3.3	1.12	
left lingual gyrus				-14	-77	0	3.6	3.38	
right lingual gyrus				18	-85	-7	3.5	2.31	
left occipital gyrus				-29	-95	13	3.5	3.88	
light occipital gyrus				14	-95	20	3.3	0.67	
reft fusiform gyrus				-29	-75	-11	3.5	1.21	
right fusiform gyrus				34	-62	-11	3.4	2.50	
cerebellum				-14	-38	-41	3.6	0.54	

* The merged Automated Anatomical Labeling was used, as introduced by PMOD (<http://doc.pmod.com/pneuro/6750.htm>), with additional small structures joined (as compared to MNI-AAL in: Tzourio-Mazoyer et al., 2002). Medial structures, including the cingulate gyrus, precuneus and cuneus were presented regardless of hemisphere.

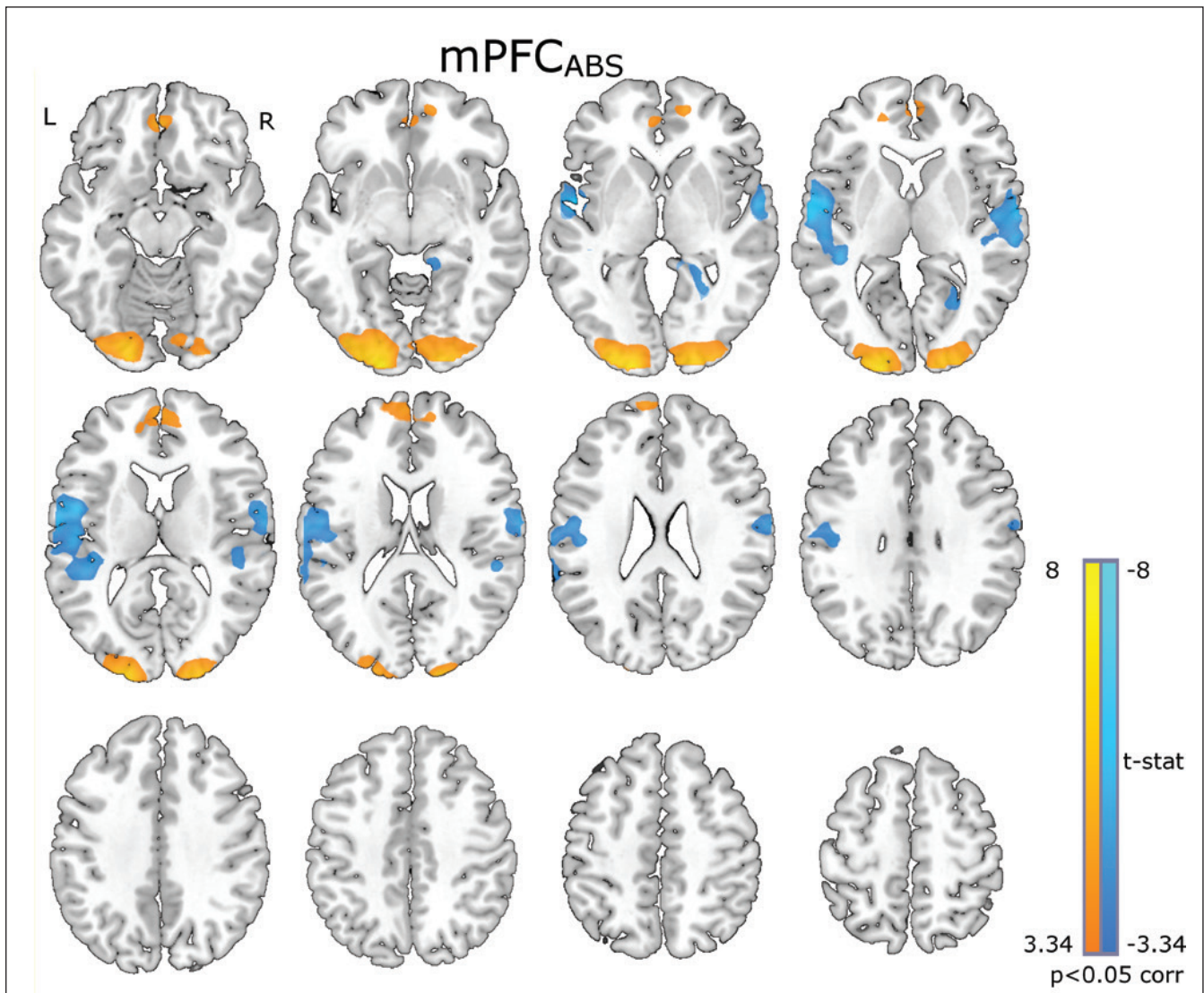


Fig. S4. Group results of the GLM analysis of fMRI data for $mPFC_{ABS}$ (contrast $mPFC_{ABS}$ vs. EC state). The yellow and blue areas represent positive and negative effects, respectively. All results were significant after AlphaSim cluster-level correction for multiple comparisons ($P < 0.05$) after passing an uncorrected threshold of $P = 0.001$.

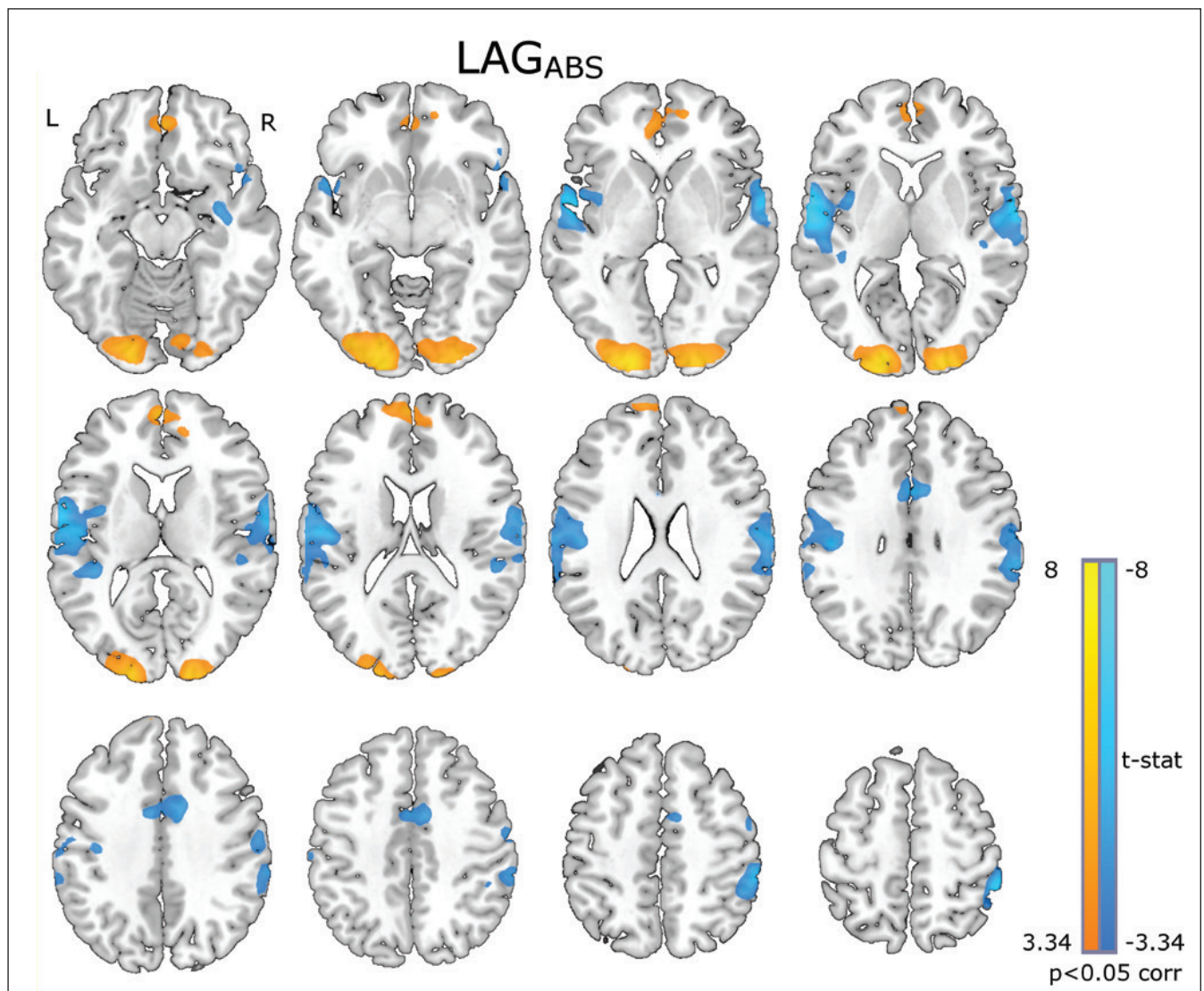


Fig. S5. Group results of the GLM analysis of fMRI data for LAG_{ABS} (contrast LAG_{ABS} vs. EC state). The yellow and blue regions represent positive and negative effects, respectively. All results were significant after AlphaSim cluster-level correction for multiple comparisons ($P < 0.05$) after passing an uncorrected threshold of $P = 0.001$.

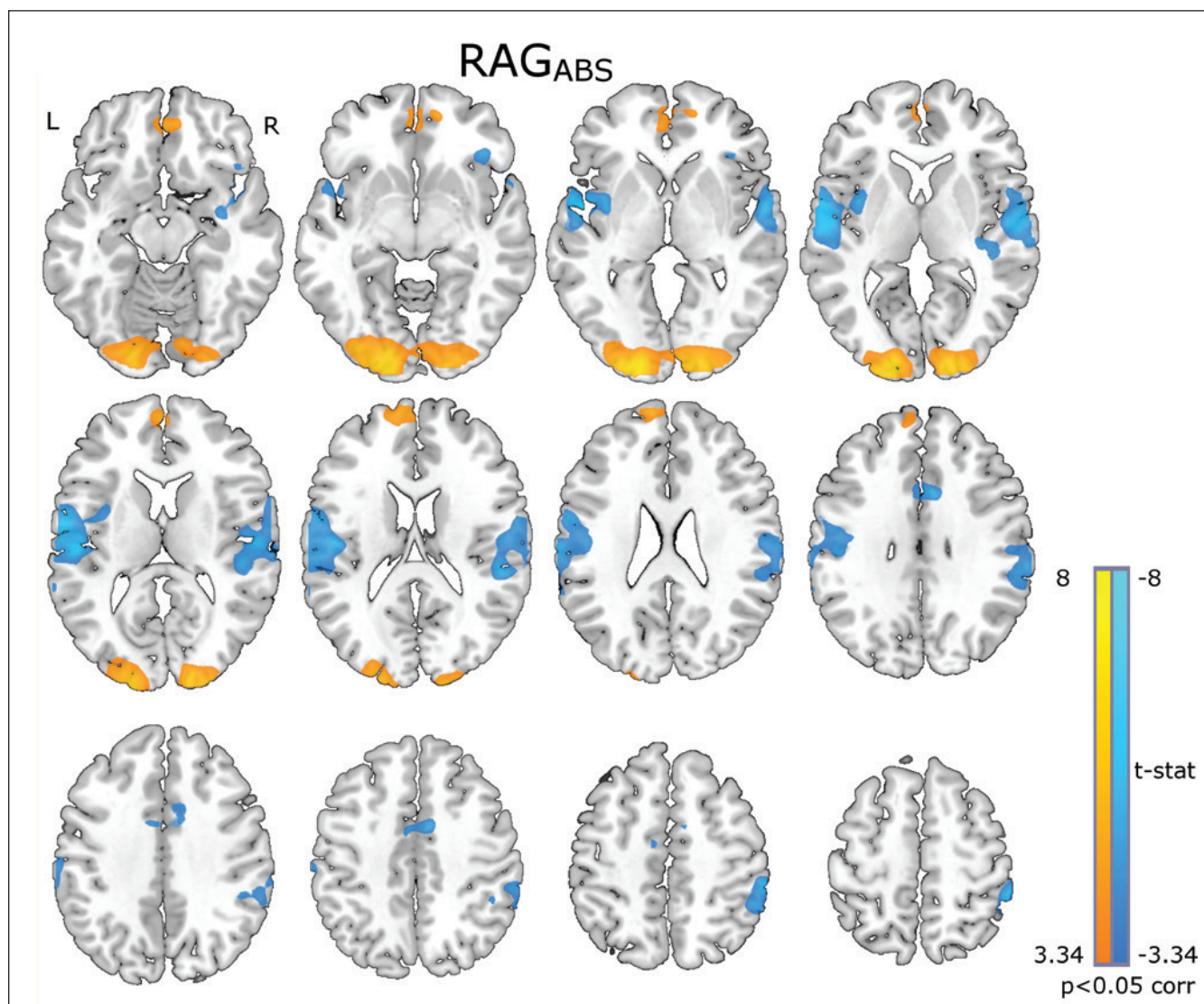


Fig. S6. Group results of the GLM analysis of fMRI data for RAG_{ABS} (contrast RAG_{ABS} vs. EC state). The yellow and blue regions represent positive and negative effects, respectively. All results were significant after AlphaSim cluster-level correction for multiple comparisons ($P < 0.05$) after passing an uncorrected threshold of $P = 0.001$.

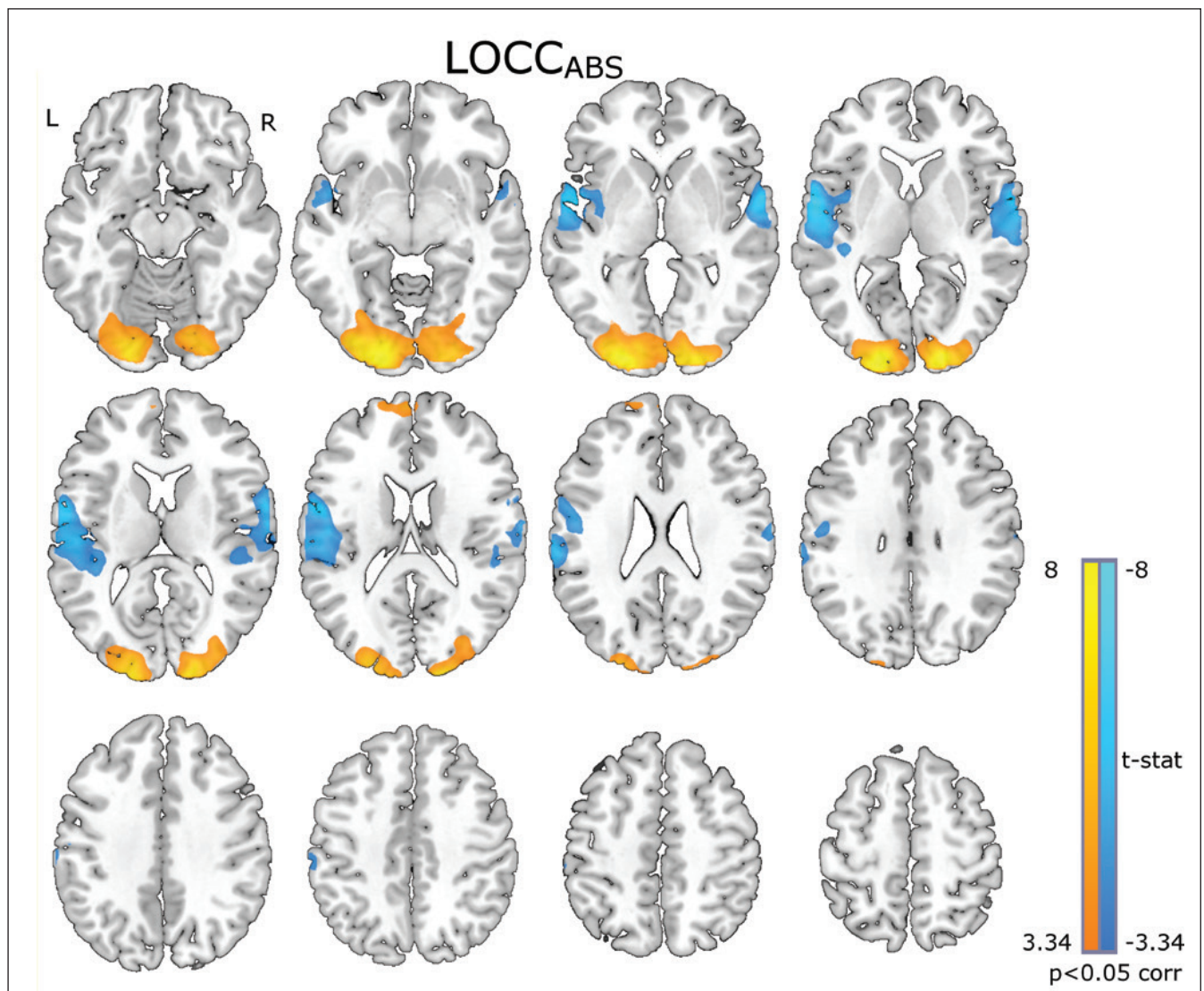


Fig. S7. Group results of the GLM analysis of fMRI data for LOCC_{ABS} (contrast LOCC_{ABS} vs. EC state). The yellow and blue regions represent positive and negative effects, respectively. All results were significant after AlphaSim cluster-level correction for multiple comparisons ($P < 0.05$) after passing an uncorrected threshold of $P = 0.001$.

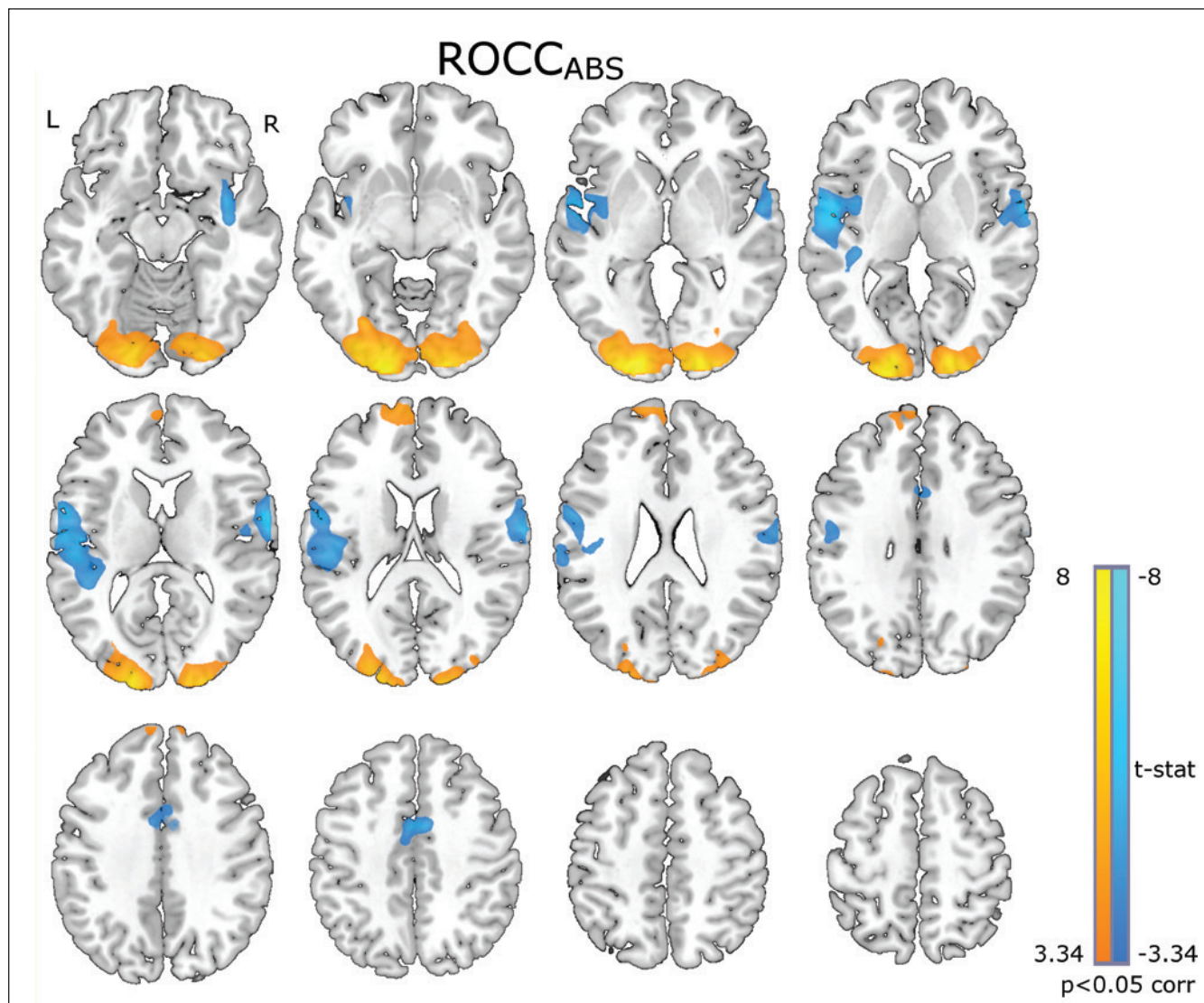


Fig. S8. Group results of the GLM analysis of fMRI data for ROCC_{ABS} (contrast ROCC_{ABS} vs. EC state). The yellow and blue regions represent positive and negative effects, respectively. All results were significant after AlphaSim cluster-level correction for multiple comparisons ($P < 0.05$) after passing an uncorrected threshold of $P = 0.001$.

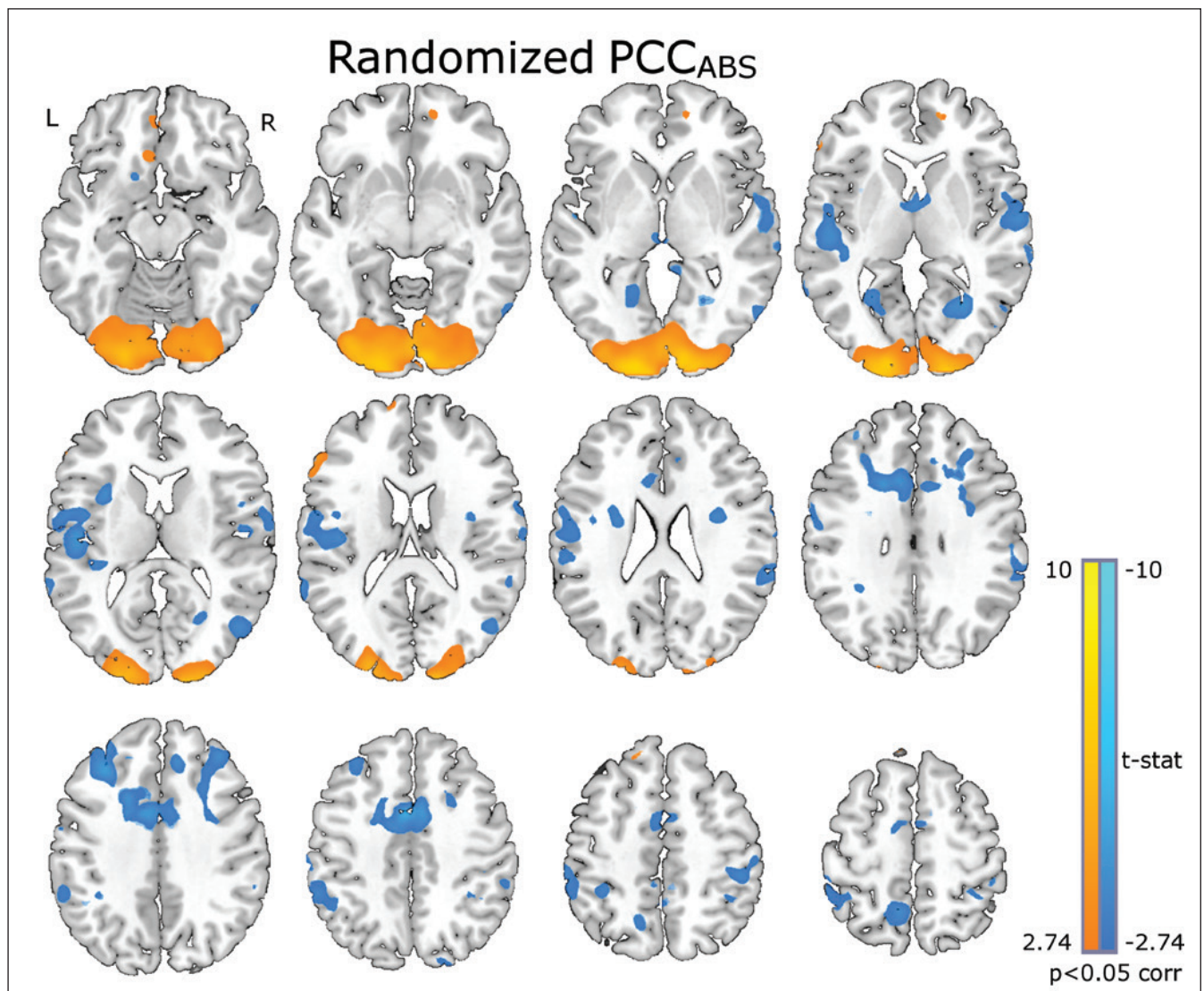


Fig. S9. Group results of the GLM analysis of fMRI data for PCCABS (contrast PCCABS vs. EC state). The ABS event vectors were randomly assigned to subject (see description in text). The yellow and blue regions represent positive and negative effects, respectively. All results were significant after cluster-level correction for multiple comparisons ($P < 0.05$) after passing an uncorrected threshold of $P = 0.005$.

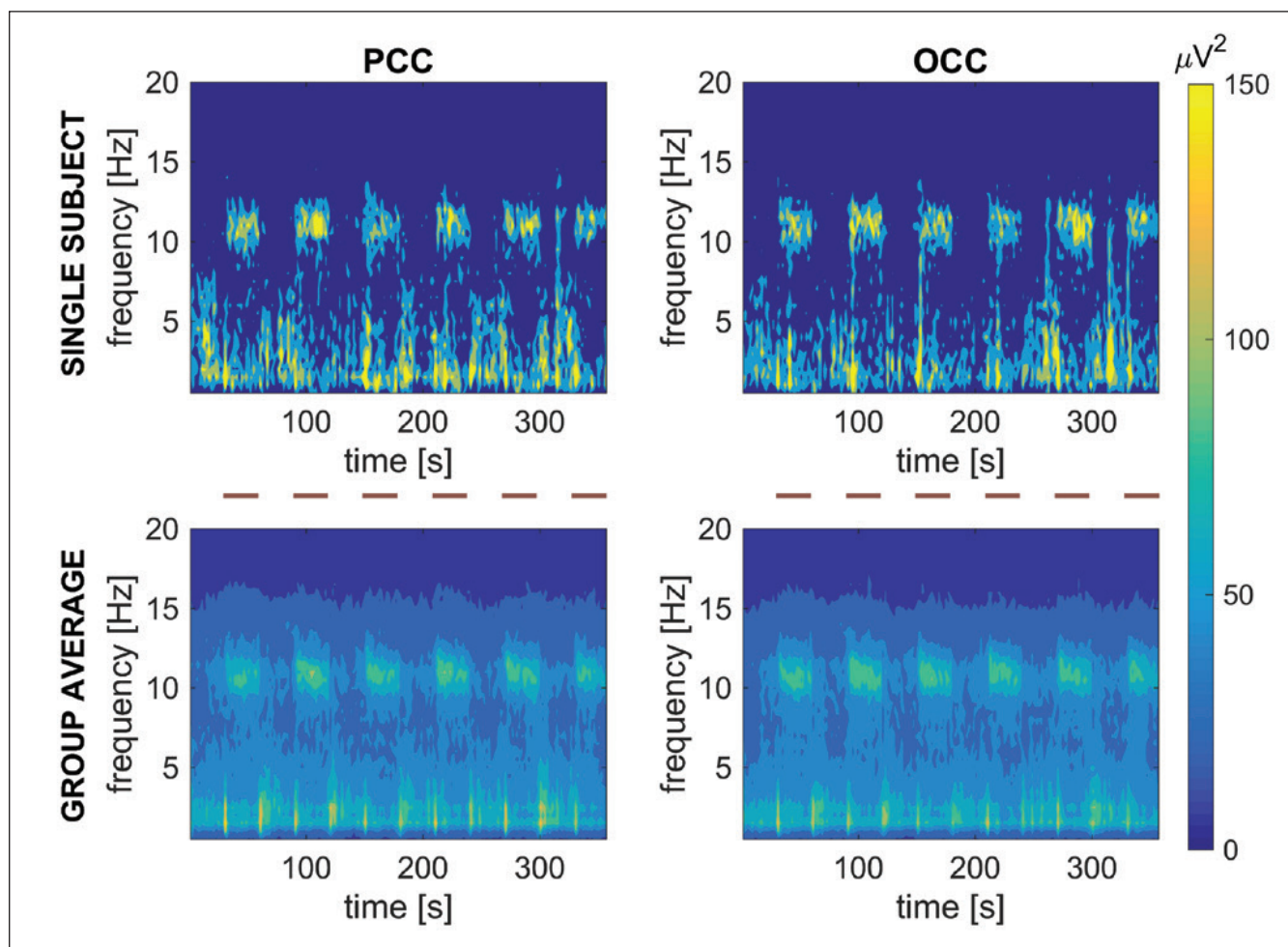


Fig. S10. Short-time Fourier transformation (STFT) of EEG data for single subject (top row) and group average (bottom row). First column: the STFT analysis results for PCC regional source; Second column: the STFT analysis results for averaged occipital regional sources: LOCC and ROCC (OCC). The time when eyes should remain closed is indicated with brown color lines. STFT was performed in 2s bin windows.